NASA TECHNICAL NOTE

NASA TN D-2678

NASA TN D-2678

EFFECTS OF UNCERTAINTIES IN THE THERMAL CONDUCTIVITY OF AIR ON CONVECTIVE HEAT TRANSFER FOR STAGNATION TEMPERATURE UP TO 30,000° K

by John T. Howe and Yvonne S. Sheaffer

Ames Research Center
Moffett Field, Calif.

NATIONAL AERONAUTICS AND SPACE ADMINISTRATION • WASHINGTON, D. C. • FEBRUARY 1965

EFFECTS OF UNCERTAINTIES IN THE THERMAL CONDUCTIVITY OF AIR ON CONVECTIVE HEAT TRANSFER FOR STAGNATION TEMPERATURE UP TO 30,000° K

By John T. Howe and Yvonne S. Sheaffer

Ames Research Center
Moffett Field, Calif.

NATIONAL AERONAUTICS AND SPACE ADMINISTRATION

For sale by the Office of Technical Services, Department of Commerce,
Washington, D.C. 20230 -- Price $2.00

EFFECTS OF UNCERTAINTIES IN THE THERMAL CONDUCTIVITY OF AIR ON CONVECTIVE HEAT TRANSFER FOR STAGNATION TEMPERATURE UP TO 30,000° K

By John T. Howe and Yvonne S. Sheaffer

Ames Research Center
Moffett Field, Calif.

SUMMARY

Convective heat transfer is examined for earth entry speeds up to 85,000 ft/sec corresponding to a stagnation region temperature of approximately 30,000° K. There is considerable uncertainty in the total thermal conductivity of air at temperatures above 15,000° K. The effect of this uncertainty on convective heat transfer is studied. Correlation formulas for the thermodynamic and transport property parameters used in the analysis are presented as functions of enthalpy for pressure levels 0.1, 1.0, and 10 atmospheres. These include density, temperature, and parameters involving viscosity, Prandtl number (for three models of total thermal conductivity), and the Planck mean mass absorption coefficient for gaseous radiation. These property correlations are presented in a form useful for digital computer programs.

INTRODUCTION

To make meaningful predictions of convective heat transfer during entry into planetary atmospheres it is necessary to know both the thermodynamic and transport properties of the reacting mixture of atmosphere and ablation gases at the high temperatures in the thin gas cap ahead of an entry vehicle. The total thermal conductivity is of particular interest. This transport property includes effects of a multitude of phenomena: ordinary translational energy transport, multicomponent diffusion of energy, thermal diffusion effects, chemical reactions, and for ionized gases, charge separation.

For air in chemical equilibrium uncontaminated by ablation vapors, the total thermal conductivity is known quite well up to temperatures of 10,000° K and fairly well up to 15,000° K. This knowledge is sufficient for predicting stagnation region convective heating for manned entry trajectories at speeds up to about 50,000 ft/sec. It is sufficient for side wall convective heating predictions for optimum conical entry body configurations at speeds up to about 90,000 ft/sec and was so employed in reference 1.

Of course, conical entry configurations will have a blunted stagnation region because of thermal erosion of the cone point. In the stagnation

region, the temperature will be 30,000° K for flight speeds between 75,000 and 85,000 ft/sec at shock layer pressure levels of 10 and 1 atmospheres as shown in figure 1.

The total thermal conductivity of air at these temperatures is not well known. Some uncertainties in the existing theoretical estimates of this property are attributable to deficiencies in knowledge of phenomena important to energy transport and of the mathematical methods used for estimating the property. Some of these difficulties are discussed in reference 2.

Thus the purpose of this paper is to evaluate the importance of the uncertainty in total thermal conductivity on convective heat transfer. To this end, three models of total thermal conductivity are employed in solving the Navier-Stokes equations in the stagnation region of blunt bodies. Correlation formulas for the appropriate thermodynamic and transport property parameters used in the analysis are presented in the appendix in the same format as that of reference 3.

SYMBOLS

$a, b, c, d, e_1, \ldots, e_n$	coefficients in equation (A1)
c_p	specific heat at constant pressure
$E_\gamma(\tau)$	function defined by $\int_1^\infty \frac{e^{-\tau w} dw}{w^\gamma}$, $\gamma = 1, 2, 3, \ldots$
f	dimensionless stream function
g	ratio of local total enthalpy to that just behind the shock wave
h	static enthalpy
j	total enthalpy
K	Planck mean mass absorption coefficient
k	total thermal conductivity
m	zero for two-dimensional flow, unity for axisymmetric flow
Pr	Prandtl number based on total specific heat and thermal conductivity
p	static pressure
q	heating rate at the surface

R	body nose radius
T	temperature
$\overline{T}$	ratio of local temperature to that just behind the shock wave
t	dummy optical depth
U	flight velocity
u	component of local flow velocity parallel to the body surface
v	component of local flow velocity normal to the body surface
y	distance normal to body surface
α_w	wall absorptivity
δ	shock-wave standoff distance
ϵ	density ratio across bow shock wave
ϵ_w	wall emissivity
μ	coefficient of viscosity
ρ	mass density
σ	Stefan-Boltzmann constant
τ	optical depth measured outward from body surface
φ	density viscosity product parameter (eq. (5))

Superscripts

$'$,$''$,$'''$	differentiation with respect to the similarity coordinate normal to the wall

Subscripts

c	convective
g	gas
r	reference conditions (corresponds to satellite enthalpy)
s	conditions immediately behind the bow shock

w conditions at the wall

∞ ambient conditions ahead of shock wave

ANALYSIS

Flow Field

The method of analysis of the flow field has been described in detail in references 4 and 5. Very briefly it consists in solving the transformed Navier-Stokes equations in the stagnation-region gas cap from the body to the shock wave. These coupled nonlinear integro-differential equations include mass, momentum, and energy transport phenomena, the last of which is expressed in terms of the total thermal conductivity of a reacting partially ionized gas and the emission and absorption of radiant energy in the gas cap and at the surface.

Assumptions employed in the analysis include: (1) The gas composition is that of local chemical equilibrium; (2) local similarity prevails in the stagnation region; (3) radiative transport is that of a plane parallel grey gas. These assumptions are evaluated in the two references cited above. They appear to be quite reasonable and lead to results that are in detailed agreement with a number of kinds of results (e.g., shock detachment distance, flow-field structure, radiative and convective heat transfer) of other analyses in regions where they overlap.

It is worth mentioning that the grey gas assumption used in conjunction with the Planck mean mass absorption coefficient leads to the identical gaseous radiative flux, energy depletion, and coupling between radiative and convective heat transfer that a spectral analysis for a nongrey gas would produce as long as gaseous reabsorption is negligible. For the examples considered, reabsorption is not severe and we can be reasonably confident of the result.

Very briefly, the transformed flow-field equations to be solved are

$$(\varphi f'')' + ff'' = \frac{1}{(m+1)}\left[(f')^2 - 2\frac{\rho_\infty}{\rho}(1-\epsilon)\right] \tag{1}$$

and

$$\left(\frac{\varphi g'}{Pr}\right)' + fg' = -\left[\frac{4R\sigma T_s^4}{(m+1)U^3}\right] K\left\{\int_0^{t_s} \overline{T}^4(t)E_1(|t-\tau|)dt - 2\overline{T}^4(\tau) + E_2(\tau)\left[\epsilon_w \overline{T}_w^4 + 2(1-\alpha_w)\int_0^{t_s} \overline{T}^4(t)E_2(t)dt\right]\right\} = Q \tag{2}$$

The energy equation (2) differs from that in references 4 and 5 in a minor way; that is, the terms in the second brackets take into account the effect of a partially reflecting wall (and reduce to the form in the references if $\epsilon_w = \alpha_w = 1$).[1]

Boundary conditions for equations (1) and (2) are

$$\left.\begin{aligned} f_w &= -\rho_w v_w \sqrt{\frac{R}{\rho_s \mu_s U(m+1)}} \\ f_w' &= 0 \\ f_s &= \rho_\infty \sqrt{\frac{RU}{\rho_s \mu_s (m+1)}} \\ f_s' &= 1 \end{aligned}\right\} \tag{3}$$

and

$$\left.\begin{aligned} g_w &= \frac{2h_w}{U^2} \\ g_s &= 1 \end{aligned}\right\} \tag{4}$$

The method for solving equations (1) and (2) subject to the boundary conditions (3) and (4) is presented in reference 4. One solution requires roughly 5 minutes of IBM 7094 digital computer time.

---

[1]The right side of equation (2) can be evaluated if the $\overline{T}^4(t)$ curve is replaced by M straight line segments in equal intervals ($\Delta t = t_s/M$) of t and the result is integrated, leading to

$$\frac{Q(\tau)}{\left[\frac{4R\sigma T_s^4}{(m+1)U^3}\right] K} = E_2(\tau)\overline{T}_w^4(\alpha_w - \epsilon_w) + \left\{E_2(|t_s - \tau|) + \frac{1}{\Delta t}\sum_{i=0}^{M-1}(\overline{T}_{i+1}^4 - \overline{T}_i^4)\left[E_3(|t_{i+1} - \tau|) - E_3(|t_i - \tau|)\right]\right\}$$

$$+ 2(1 - \alpha_w)E_2(\tau)\left\{E_3(t_M) + \frac{1}{\Delta t}\sum_{i=0}^{M-1}(\overline{T}_{i+1}^4 - \overline{T}_i^4)\left[E_4(t_{i+1}) - E_4(t_i)\right]\right\}$$

Each of the braces can be evaluated by methods presented in appendix A of reference 4.

The thermodynamic and transport property parameters needed for solving the equations are $1/\rho$, K,

$$\varphi = \frac{\rho\mu}{\rho_s\mu_s} \tag{5}$$

$$\frac{\varphi}{Pr} = \frac{\rho\mu/\rho_s\mu_s}{Pr} \tag{6}$$

and

$$\bar{T} = \frac{T}{T_s} \tag{7}$$

Correlation formulas used in the analysis for expressing ρ, K, T, $\rho\mu$, and $\rho\mu/Pr$ as functions of enthalpy at constant pressure are presented in the appendix.

In equation (6), the Prandtl number

$$Pr = \frac{c_p\mu}{k} \tag{8}$$

contains the total thermal conductivity k. It is the effects of the uncertainty in k on the solutions of equations (1) and (2) and thus on convective heat transfer that we seek.

Total Thermal Conductivity

The total thermal conductivity for air is well known through temperatures where dissociation is completed (approximately 10,000° K - fig. 1). However, at higher temperatures, where ionization occurs, there is considerable disagreement in total thermal conductivity among the various studies. Figure 2 shows that at 15,000° K, the total thermal conductivity at a pressure of 1 atmosphere predicted by Hansen (ref. 6) is almost six times that predicted by Yos (ref. 7) and is only about half that obtained experimentally by Maecker (ref. 8) in nitrogen. In spite of the fact that this early result of Hansen did not include the very important effects of charge exchange, it has in its favor reasonable agreement with the Maecker arc data (at temperatures up to 14,500° K) and the fact that it leads to predictions of convective heat transfer that agree fairly well with experimental results (ref. 9). Moreover, experimental results of Michel Chen[2] of Yale University agree with those of Maecker (within experimental error) at temperatures up to 14,000° K. Chen analyzed his arc data in a way different from that of Maecker, avoiding the uncertainties and difficulties associated with spectroscopic analysis of nonuniform gas samples. The more recent theoretical result of Yos is on a firmer phenomenological basis than that of Hansen in that it does account for effects of charge exchange in the reactive component of total thermal conductivity.

[2]In a private communication.

However, the still more recent work of Knof, Mason, and Vanderslice (ref. 10) show charge exchange cross sections that are only about 1/3 those of Delgarno (ref. 11) on which Yos' estimates were based. These new cross-section estimates agree well with recent experimental results of Stebbings, according to reference 10. The implication is that Yos' estimate of total thermal conductivity may be too low; specifically, the reactive component may be too low by a factor of 3. It may also be too low because of other effects, such as the neglect of higher order terms, charge separation, and thermal diffusion. For example, the second-order Chapman-Enskog analysis by Ahtye (ref. 2) leads to a translational thermal conductivity that is larger than that of the first-order approximation by 30 to 50 percent at half and full single ionization, respectively, and 100 percent at double ionization. Moreover, because the effects of charge separation on concentration gradients of ions and electrons are still unknown, the other two components (reactive and thermal diffusive) of thermal conductivity have yet to be estimated meaningfully.

Thus total thermal conductivity at temperatures above 10,000° K is somewhat uncertain and above 15,000° K is very uncertain. To the knowledge of the authors, there exist neither experimental values for total thermal conductivity nor convective heat-transfer results which may be used to verify theoretical total thermal conductivity estimates at temperatures above 15,000° K.

In order to examine the effects of these uncertainties at high temperatures on convective heat transfer, we employ three models of total thermal conductivity designated by Roman numerals I, II, III in figure 2. The first of these (I) is that of Yos shown by the bottom curve in the figure. The second (II) was obtained by raising the high temperature end of the Yos estimates by roughly an order of magnitude (actually a factor of about 8 at 15,000° K, a factor of 10 or more from 16,000° to 24,000° K, and about 9 at 30,000° K) and is shown by the top curve. This curve represents an arbitrary increase of the Yos result and is not a phenomenological upper limit. It agrees with both the Maecker data and Hansen's results reasonably well at temperatures up to 14,500° K. The third model (III) may be thought of loosely as the Hansen result faired into the Yos result. It is the intermediate curve, which was obtained by modifying the reactive part of the Yos result in the single ionization regime by use of elastic cross sections of nitrogen rather than charge exchange cross sections, simply to provide a prominent peak in the single ionization region. The convective heating results corresponding to these three total thermal conductivity models will also be identified by the Roman numerals.

RESULTS AND DISCUSSION

Convective Heat Transfer

The stagnation region convective heating results obtained from flow-field solutions employing the three models of total thermal conductivity are shown in figure 3. All results exclude mass addition effects (f_w in boundary condition (3) is zero). They correspond to Reynolds numbers (defined as

$\rho_s R\sqrt{j_s}/\mu_s$) of approximately 10^5 so that vorticity near the shock probably does not significantly influence convective heating rates at the wall. Radiative depletion of flow-field energy was small (because small nose radii, from 0.25 to 0.5 ft, and relatively low radiative properties were used - see appendix) and had a negligible effect on convective heat transfer. At a speed of 70,000 ft/sec, the highest model of total thermal conductivity (II) leads to a convective heating rate which exceeds that of the lowest model (I) by a factor 1.75, while at 85,000 ft/sec, the factor is approximately 2. This is in spite of a difference of an order of magnitude in the total thermal conductivity models above 15,000° K.

The convective heating result of reference 4 (without radiative coupling) is shown for flight speed up to 50,000 ft/sec by the long-dash line. If this line is simply extended to higher speed (the dot-dash line), we see that the deviation from it at 70,000 ft/sec is only 20 percent above and 30 percent below for the two extreme models, while at 85,000 ft/sec the deviation is about 40 percent in each direction. An extrapolation of the convective heating result of Hoshizaki (ref. 12) by use of his convective heating correlation formula lies close to the extrapolation of reference 4.

The reason for the insensitivity of convective heating rate to large changes in total thermal conductivity at high temperatures is simple. For problems of practical interest, the wall temperature is low (about 3,000° K) relative to that behind the bow shock wave (about 30,000° K). Thus a region of relatively cold gas exists adjacent to the wall. In that region, total thermal conductivity is the same in all cases. The differences in the total thermal conductivity models occur some distance away from the wall, in that part of the flow field where the temperature exceeds 10,000° K. A change in thermal conductivity in the outer region can only indirectly affect convective heating at the surface by changing the over-all enthalpy profile and thus modifying its gradient at the surface. In this way the relatively cool layer adjacent to the wall acts as a cushion to soften the influence of the effects in the outer flow region on the wall itself.

Flow Field

The flow-field profiles corresponding to the three models of total thermal conductivity for flight speed of 70,000 ft/sec are shown in figures 4, 5, and 6.

It is seen that there is little influence of the uncertainty in thermal conductivity on the velocity profile. This is to be expected in view of the general weak coupling of the momentum equation to the energy equation mentioned in reference 4. The Reynolds number ($\rho_s R\sqrt{j_s}/\mu_s$) is approximately 10^5 and a momentum boundary layer of about 20 percent of the flow field is clearly evident in the u/u_s profiles.

On the other hand, a comparison of figures 4 and 5, which correspond to the extremes in thermal conductivity, shows strong influence of the uncertainty in thermal conductivity on the enthalpy profiles (j/j_s). (It has already been noted that radiative depletion of flow-field energy is small for these examples.) Thus for the low thermal conductivity of Yos, 65 percent of the flow field is essentially isoenergetic and a thermal boundary layer of 35 percent of the flow field is evident in the j/j_s profile of figure 4. By comparison, the high thermal conductivity result of figure 5 shows the flow field to be nonisoenergetic everywhere, and the thermal boundary layer is less sharply defined. The transport property parameter, φ/Pr, responsible for the differences in the enthalpy profiles is also shown in figures 4 and 5.

The effects of total thermal conductivity on flow-field solutions at 85,000 ft/sec can be seen by comparing figures 7 and 8, corresponding to the two extreme models (I and II) of total thermal conductivity. Here the effects on the enthalpy profile are greater than those at 70,000 ft/sec, as would be expected, and it can be noted that even the relatively insensitive velocity profiles are affected.

Of course, the uncertainty in total thermal conductivity which affects the energy structure of the flow field also influences the gaseous radiative flux at the surface, 30 percent for both the 70,000 and 85,000 ft/sec examples (as calculated from flow-field solutions).

CONCLUSIONS

Solutions of the stagnation region Navier-Stokes equations have been obtained for flight speeds up to 85,000 ft/sec and shock-layer temperatures up to 30,000° K. Convective heat-transfer rates have been derived from the solutions.

An uncertainty of a factor of 10 in total thermal conductivity of air at temperatures above 15,000° K influences the convective heating rate by only a factor of 1.75 at a flight speed of 70,000 ft/sec and by a factor of 2 at 85,000 ft/sec. This insensitivity of convective heating rate is a consequence of a layer of relatively cool gas adjacent to the surface which cushions the effects of the uncertainties of the behavior of the hot gas farther from the wall.

The uncertainty in total thermal conductivity influences the energy structure of the hot part of the flow field. Consequently, for the examples studied, the gaseous radiative flux at the surface is influenced almost as importantly as the convective flux.

Apparently, it is important to improve our knowledge of total thermal conductivity of partially ionized air to within about a factor of 2 at temperatures above 15,000° K from the practical point of view of convective and radiative heating of stagnation regions. Moreover, it is generally important

that a better understanding of the physical and chemical processes of partially ionized gas mixtures be acquired, and out of this an improved understanding of transport properties is bound to emerge.

Ames Research Center
National Aeronautics and Space Administration
Moffett Field, Calif., Oct. 27, 1964

APPENDIX A

THERMODYNAMIC AND TRANSPORT PROPERTY CORRELATION FORMULAS FOR EQUILIBRIUM AIR FROM 3,000° to 30,000° K

The quantities ρ, $\rho\mu$, $\rho\mu/Pr$, T, and K as functions of h at constant pressure are required for solving the differential equations (1) and (2). These properties, which we want to represent by correlation formulas, have been normalized with respect to their values (see table I) at a reference enthalpy h_r (arbitrarily selected to be satellite enthalpy 3.125×10^8 ft^2/sec^2 or 12,474 Btu/lb_m) and are shown as open symbols in figures 9 through 23.

These quantities were obtained from information from a number of sources. The thermodynamic quantities T, ρ, and c_p were obtained from Ahtye and Peng (ref. 13). The viscosity, μ, and total thermal conductivity, k, were obtained from Yos (ref. 7). The values for μ and k at 0.1 atm were obtained by extrapolating Yos' result in terms of the $\log_{10}$ of pressure using his 100, 10, and 1 atm results. At 1 atm pressure, of course, two other models of k were employed as discussed previously. The Planck mean mass absorption coefficient, K, was obtained from two sources; Kivel and Bailey (ref. 14), and Armstrong, Sokoloff, Nicholls, Holland, and Meyerott (ref. 15). At temperatures up to 8,000° K (for which the two references are in substantial agreement), the result of Kivel and Bailey was used. For temperatures from 8,000° to 30,000° K (for which Kivel and Bailey[1] are higher than Armstrong et al. by as much as a factor of 4) the result of Armstrong et al. was used.

Each property represented by the symbols was correlated at each of three pressure levels, 0.1, 1.0, and 10 atmospheres,[2] by the general expression

$$a + bz + cz\,\frac{h}{h_r} + dz^2 + e_1\,\frac{h}{h_r} + e_2\left(\frac{h}{h_r}\right)^2 + e_3\left(\frac{h}{h_r}\right)^3, \ldots, e_n\left(\frac{h}{h_r}\right)^n = 0 \qquad (A1)$$

for temperatures between 3,000° and 30,000° K. The symbol z represents the property in question normalized with respect to its value at reference enthalpy. The lines in figures 9 through 23 are the result of the correlation formula (A1), whose coefficients a, b, c, d, e_1, . . . , e_n are listed in table II. It can be seen in the table that some of the curves have been broken into several segments and that different coefficients apply to different segments.

---

[1]The upper limit of the Kivel and Bailey result is 18,000° K.

[2]At 1 atmosphere pressure, there are three sets of correlation formulas for the quantity $(\rho\mu/Pr)/(\rho_r\mu_r/Pr_r)$ corresponding to the three models of total thermal conductivity shown previously in figure 2.

Equation (A1) includes two general types of curves. Thus if the coefficients $e_3, \ldots, e_n$ are zero, the equation is that of a general conic with inclined axis. If c and d are zero, the equation is that of a polynomial of degree n.

Using this means of correlating thermodynamic and transport properties is economical of computer time; that is, an eighth degree polynomial can be evaluated at 10,000 points in approximately one second by an IBM 7094 data processing machine.

REFERENCES

1. Chapman, Gary T.: Theoretical Laminar Convective Heat Transfer and Boundary-Layer Characteristics on Cones at Speeds to 24 km/sec. NASA TN D-2463, 1964.

2. Ahtye, Warren F.: A Critical Evaluation of Methods for Calculating Transport Coefficients of a Partially Ionized Gas. Proc. 1964 Heat Transfer and Fluid Mech. Inst., Stanford Univ. Press, 1964.

3. Viegas, John R., and Howe, John T.: Thermodynamic and Transport Property Correlation Formulas for Equilibrium Air From 1000° K to 15,000° K. NASA TN D-1429, 1962.

4. Howe, John T., and Viegas, John R.: Solutions of the Ionized Radiating Shock Layer, Including Reabsorption and Foreign Species Effects, and Stagnation Region Heat Transfer. NASA TR R-159, 1963.

5. Howe, John T., and Sheaffer, Yvonne S.: Mass Addition in the Stagnation Region for Velocity up to 50,000 Feet per Second. NASA TR R-207, 1964.

6. Hansen, C. Frederick: Approximations for the Thermodynamic and Transport Properties of High-Temperature Air. NASA TR R-50, 1959.

7. Yos, Jerrold M: Transport Properties of Nitrogen, Hydrogen, Oxygen, and Air to 30,000° K. AVCO Rep. RAD TM 63-7, 1963.

8. Maecker, H.: Thermal and Electrical Conductivity of Nitrogen Up to 15,000° K by Arc Measurements. Presented at meeting on Properties of Gases at High Temperatures. AGARD, Aachen, Sept. 21-23, 1959.

9. Goodwin, Glen, and Howe, John T.: Recent Developments in Mass, Momentum, and Energy Transfer at Hypervelocities. NASA SP 24, 1962.

10. Knof, Hans, Mason, E. A., and Vanderslice, J. T.: Interaction Energies, Charge Exchange Cross Sections and Diffusion Cross Sections for N^+-N and O^+-O Collisions. Univ. of Maryland Institute for Molecular Physics IMP NASA 35, 1963.

11. Delgarno, A.: The Mobilities of Ions in Their Parent Gases. Phil Trans. Roy. Soc. London, vol. 250, series A, 1958, pp. 426-439.

12. Hoshizaki, H.: Heat Transfer in Planetary Atmospheres at Supersatellite Speeds. ARS 2173-61, ARS Jour., vol. 32, Oct. 1962, pp. 1544-51.

13. Ahtye, Warren F., and Peng, Tzy-Cheng: Approximations for the Thermodynamic and Transport Properties of High-Temperature Nitrogen With Shock-Tube Applications. NASA TN D-1303, 1962.

14. Kivel, B., and Bailey, K.: Tables of Radiation From High Temperature Air. Res. Rep. 21, AVCO Res. Lab., Dec. 1957.

15. Armstrong, B. H., Sokoloff, J., Nicholls, R. W., Holland, D. H., and Meyerott, R. E.: Radiative Properties of High Temperature Air. J. Quant. Spectrosc. Radiat. Transfer, vol. 1, no. 2, Nov. 1961, pp. 143-162.

TABLE I.- REFERENCE CONDITIONS

	p = 0.1 atm	p = 1.0 atm	p = 10.0 atm
h_r, ft^2/sec^2	3.125×10^8	3.125×10^8	3.125×10^8
ρ_r, $slugs/ft^3$	6.271×10^{-6}	5.7×10^{-5}	5.185×10^{-4}
$\rho_r \mu_r$, $lb^2 sec^3/ft^6$	2.47×10^{-11}	2.47×10^{-10}	2.47×10^{-9}
Pr_r	0.6958	1.008	0.9537
T_r, ^oK	6400	7200	8150
K_r, $ft^2/slug$	24	65	300

TABLE II.- CORRELATION FORMULA COEFFICIENTS

Thermal conductivity model	Property, z	Pressure level, atm	Type of curve (1)	h/h$_r$ limits for curve: lower	upper	a	b	c	d	e$_1$	e$_2$	e$_3$	e$_4$	e$_5$	e$_6$	e$_7$	e$_8$	e$_9$	e$_{10}$	e$_{11}$	Sign of root of quadratic
	ρ_r	0.1	P	0.037	8.0	-1.0277498-1	-1.0	0	0	4.4888099	-1.124452+1	1.4582273+1	-1.0020748+1	4.0689813	-1.0244075	1.6136825-1	-1.5449581-2	8.2099969-4	-1.8555588-5		+
				8.0	15.63	3.7673303+3	-1.0	0	0	-2.8137711+3	9.1050310+2	-1.6651766+2	1.8835756+1	-1.3497494	5.9851766-2	-1.5019387-3	1.6335417-5				+
		1.0	P	.037	6.08	1.8424094-3	-1.0	0	0	2.4478014	-3.1665066	1.6047689	8.4249593-1	-1.2801588	6.1948853-1	-1.5954459-1	2.3424577-2	-1.8545819-3	6.1622605-5		+
				6.08	12.19	1.2632851+4	-1.0	0	0	-1.1173252+4	4.2845578+3	-9.3095145+2	1.2546249+2	-1.0745014+1	5.7133986-1	-1.7250886-2	2.2651790-4				+
		10.0	P	.037	8.69	3.9827824-4	-1.0	0	0	2.1999733	-2.3973665	1.0564214	5.9174627-1	-7.7178752-1	3.4159296-1	-8.2937150-2	1.2063128-2	-1.0477777-3	5.0140753-5	-1.0172610-6	+
	$\frac{\rho\mu}{\rho_r\mu_r}$	.1	C	.037	6.29	1.0	-9.4310240-1	3.6059286-2	2.2190800-1	-3.1069500-1	2.4604797-2										-
			P	6.29	15.63	2.9637247-2	-1.0	0	0	-4.1545442-4											+
		1.0	C	.037	7.63	1.0	-9.3719251-1	-2.3410905-2	2.1995978-1	-2.5643856-1	1.6854411-2										-
			P	7.63	12.19	2.0141641-2	-1.0	0	0	2.6060358-4											+
		10.0	C	.037	8.69	1.0	-8.9096756-1	-8.4148120-2	2.0107645-1	-2.4149899-1	1.5538210-2										-
III	$\frac{\rho\mu Pr_r}{\rho_r\mu_r Pr}$	.1	C	.124	15.63	1.0	2.6298819-1	-2.6642972	-1.6993146-2	7.4862581-1	-4.7742189-2										-
		1.0	C	.124	12.19	1.0	1.1083793-2	-1.2593215	-9.1903661-3	6.2680411-1	-5.2146950-2										-
		10.0	C	.169	8.69	1.0	-8.8023096-2	-1.3331034	1.8572078-2	8.5181654-1	-7.2605629-2										-
	$\frac{T}{T_r}$	.1	P	.037	3.0	-9.5849097-2	-1.0	0	0	7.0269715	-2.3528511+1	4.7538562+1	-6.0405999+1	4.9130768+1	-2.5608553+1	8.4680093	-1.7141432	1.9357599-1	-9.3383289-3		+
			P	3.0	6.0	1.6977952	-1.0	0	0	-6.0021507-1	4.6471613-1	-1.1928356-1	1.3133927-2	-4.7094748-4							+
			P	6.0	8.0	2.8676416+3	-1.0	0	0	-2.0038633+3	5.5771441+2	-7.7267437+1	5.3326116	-1.4674009-1							+
			P	8.0	15.63	-1.2083204+2	-1.0	0	0	7.2458982+1	-1.8196670+1	2.5462501	-2.1396711-1	1.0795265-2	-3.0282474-4	3.6457887-6					+
		1.0	P	.037	4.0	-1.0530651-2	-1.0	0	0	4.3967872	-8.0777498	7.3891817	-3.5151263	9.0831419-1	-1.2160186-1	6.6302443-3					+
			P	4.0	8.0	-6.2961954+2	-1.0	0	0	8.3938254+2	-4.7185469+2	1.4535426+2	-2.6488069+1	2.8547189	-1.6843932-1	4.1973355-3					+
			P	8.0	12.19	-9.1008916	-1.0	0	0	4.5325111	-6.6098617-1	4.9323900-2	-1.8181287-3	2.6147644-5							+
		10.0	P	.037	8.69	-1.8822670-2	-1.0	0	0	3.9745670	-6.7428784	5.9422495	-2.8562406	8.1102968-1	-1.4021619-1	1.4510000-2	-8.2585710-4	1.9870017-5			+
	$\frac{K}{K_r}$	.1	C	.037	2.56	0	5.6196848+1	-3.1788362+1	1.0	-3.7330665+1	1.5541062+1										+
			P	2.56	7.09	-8.0847766+2	-1.0	0	0	1.1924928+3	-7.5674655+2	2.8358553+2	-6.9000565+1	1.1120773+1	-1.1465370	6.8146568-2	-1.7647153-3				+
			P	7.09	15.63	1.6865213+2	-1.0	0	0	-6.3832573+1	1.1041413+1	-9.4714031-1	4.0762839-2	-7.0342901-4							+
		1.0	C	.037	2.0	0	4.0277180+2	-1.6811143+2	1.0	-1.9286413+2	-9.0168294+1										+
			P	2.0	6.0	-3.8898747+3	-1.0	0	0	8.0879290+3	-7.4139898+3	3.9637724+3	-1.3683187+3	3.1910007+2	-5.1009413+1	5.5314012	-3.9030489-1	1.6215491-2	-3.0167195-4		+
			P	6.0	12.19	4.0345103+3	-1.0	0	0	-3.6721542+3	1.4066092+3	-2.9161676+2	3.5437826+1	-2.5306483	9.8552916-2	-1.6177253-3					+
		10.0	C	.037	3.0	0	2.3721343+1	-1.6762421+1	1.0	-2.3063969+1	1.4530446+1										+
	η		P	3.0	8.69	5.3177329+2	-1.0	0	0	-8.0959020+2	5.0990549+2	-1.6961861+2	3.2873446+1	-3.7225061	2.2787713-1	-5.8158004-3					+
I	$\frac{\rho\mu Pr_r}{\rho_r\mu_r Pr}$	1.0	C	.124	12.19	1.0	-9.6995737-2	-8.0122758-1	2.9732389-3	-1.6091295-2	-1.5145274-3										-
		1.0	C	.124	4.45	1.0	1.2143997-1	-1.6061748	-2.2607421-2	9.0477487-1	3.2725662-2										-
II			C	4.45	6.5	0	1.9526986+1	-3.5747017	1.0	-3.3118345	5.6357265-1										+
			P	6.5	7.3	-1.6805131+4	-1.0	0	0	1.8569795+4	-7.2585844+3	1.3256021+3	-1.1588564+2	3.9299821							+
			C	7.3	12.19	1.0	4.8783706	-6.7006218-1	-9.5276214-2	-1.6619748-1	1.7456592-2										-

(1) P - polynomial; C - conic.

Note: A group of digits followed by -n indicates that the decimal point should be n places to the left.

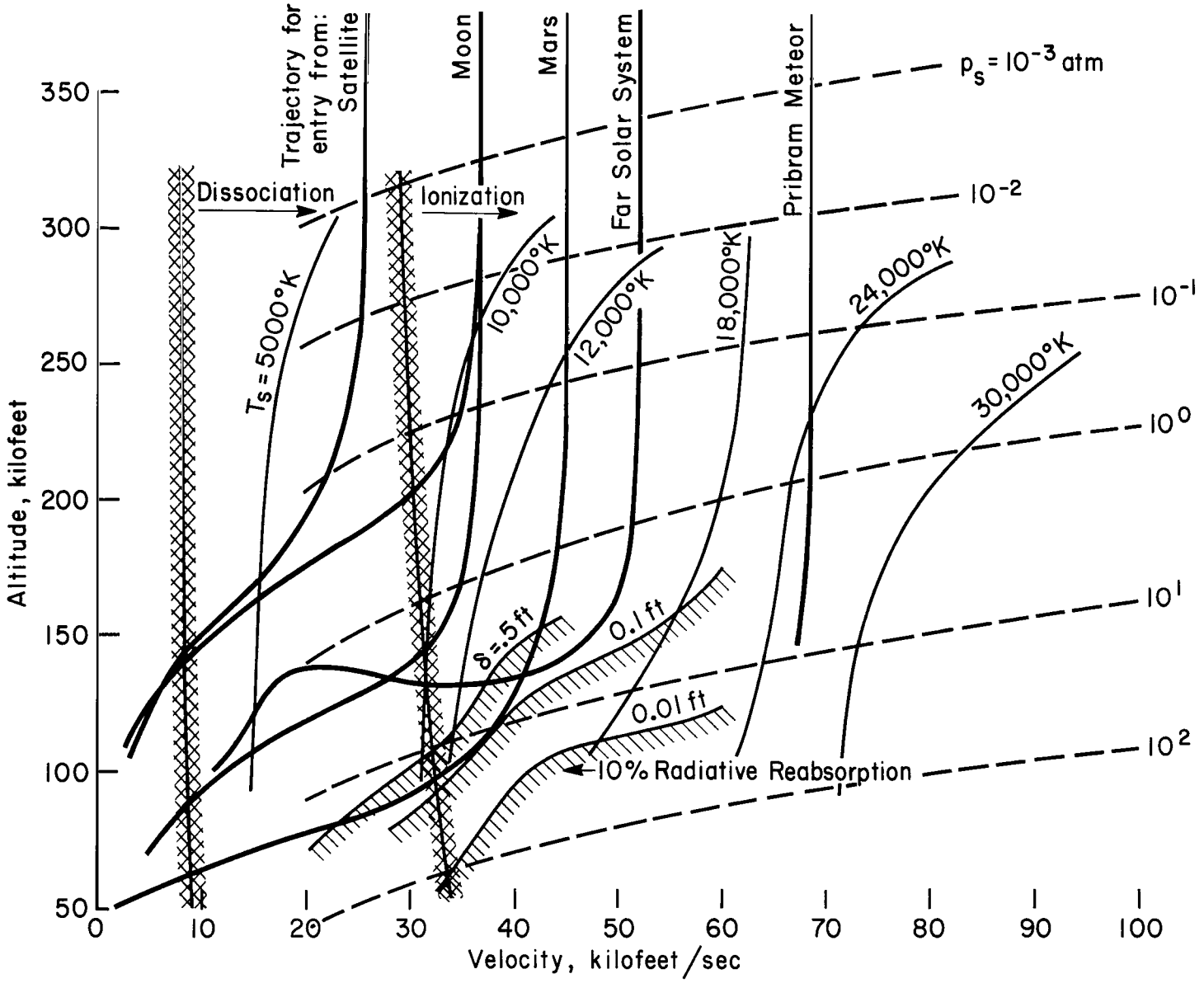

Figure 1.- Flight regime information.

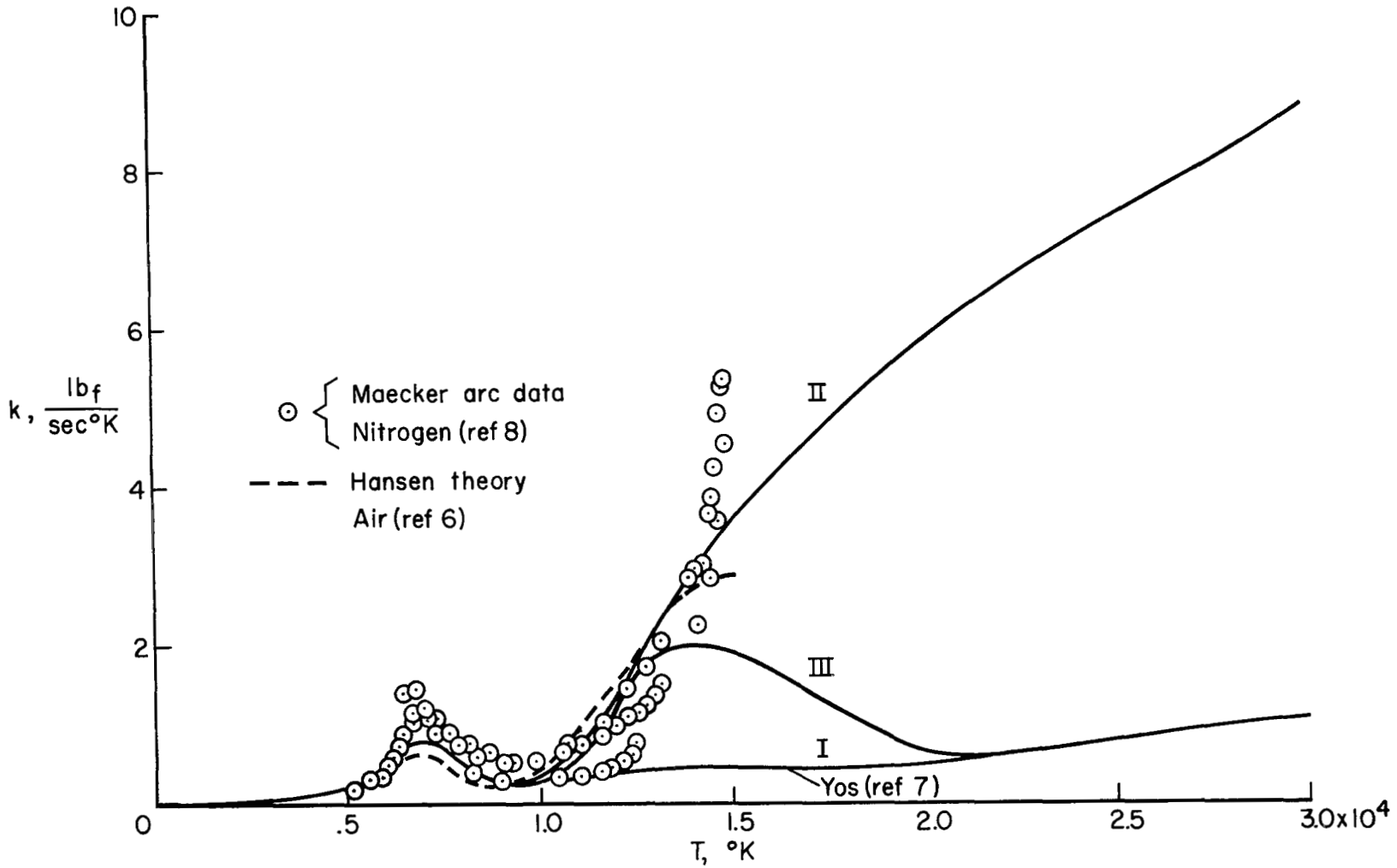

Figure 2.- Total thermal conductivity of air at one atmosphere.

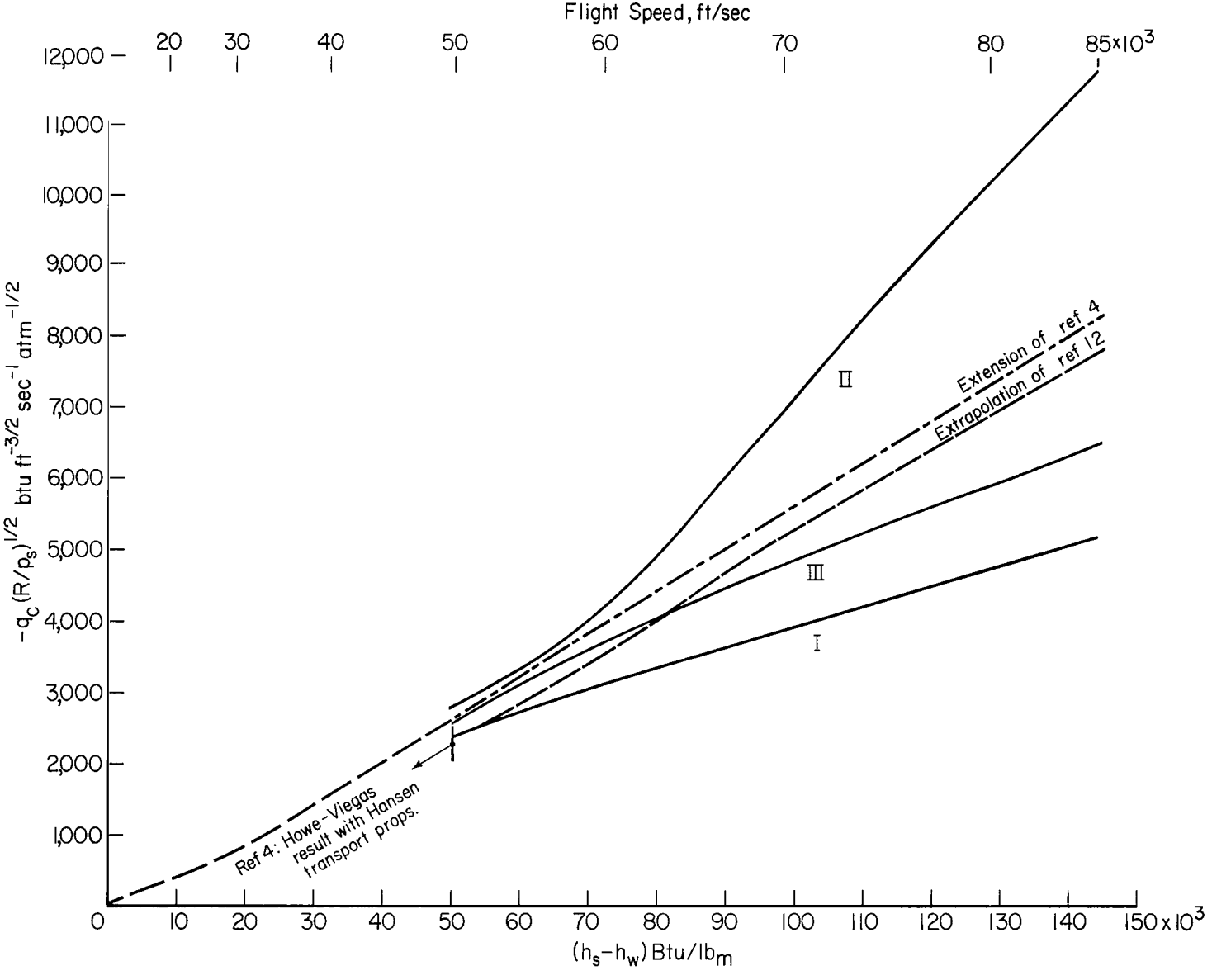

Figure 3.- Convective heating-rate results, p_s = 1 atm.

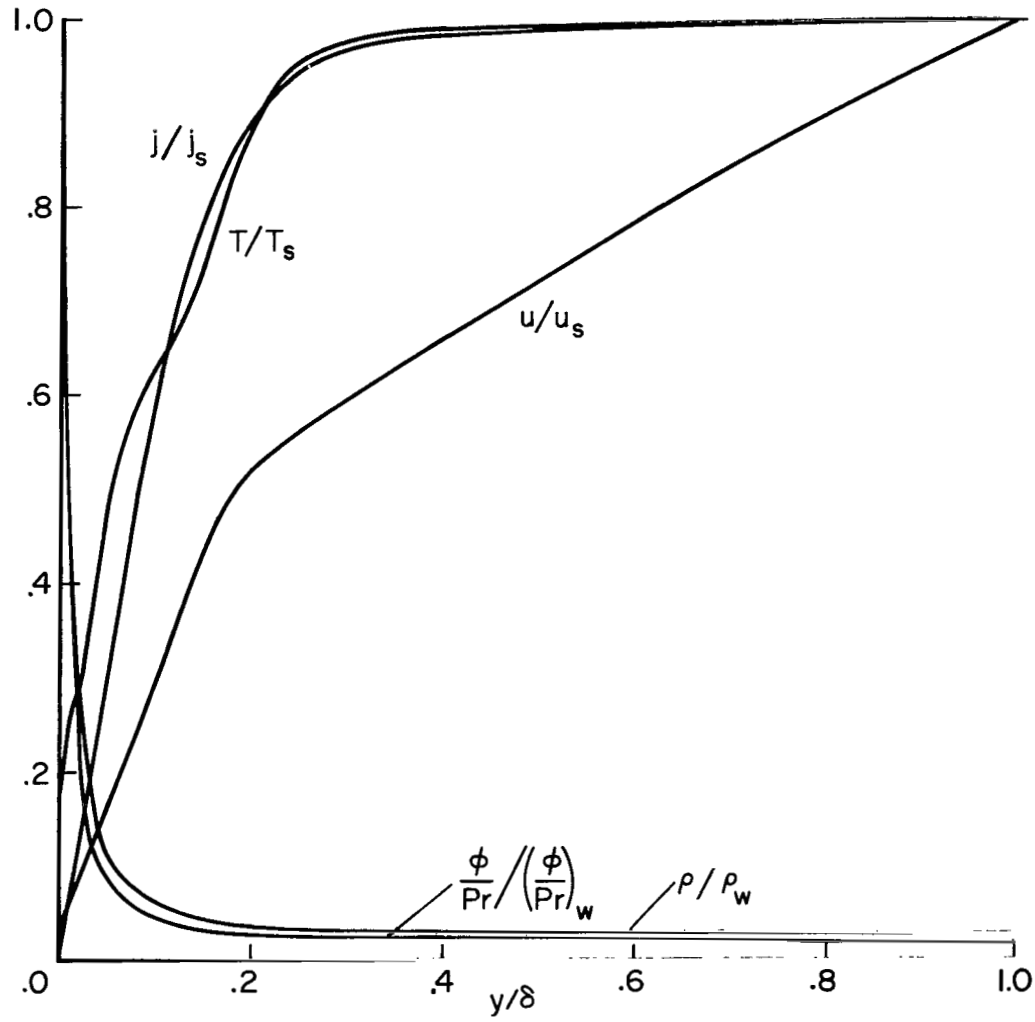

Figure 4.- Flow-field profiles for total thermal conductivity model I; U = 70,000 ft/sec, R = 0.25 ft, p_s = 1 atm, T_w = 3,000° K.

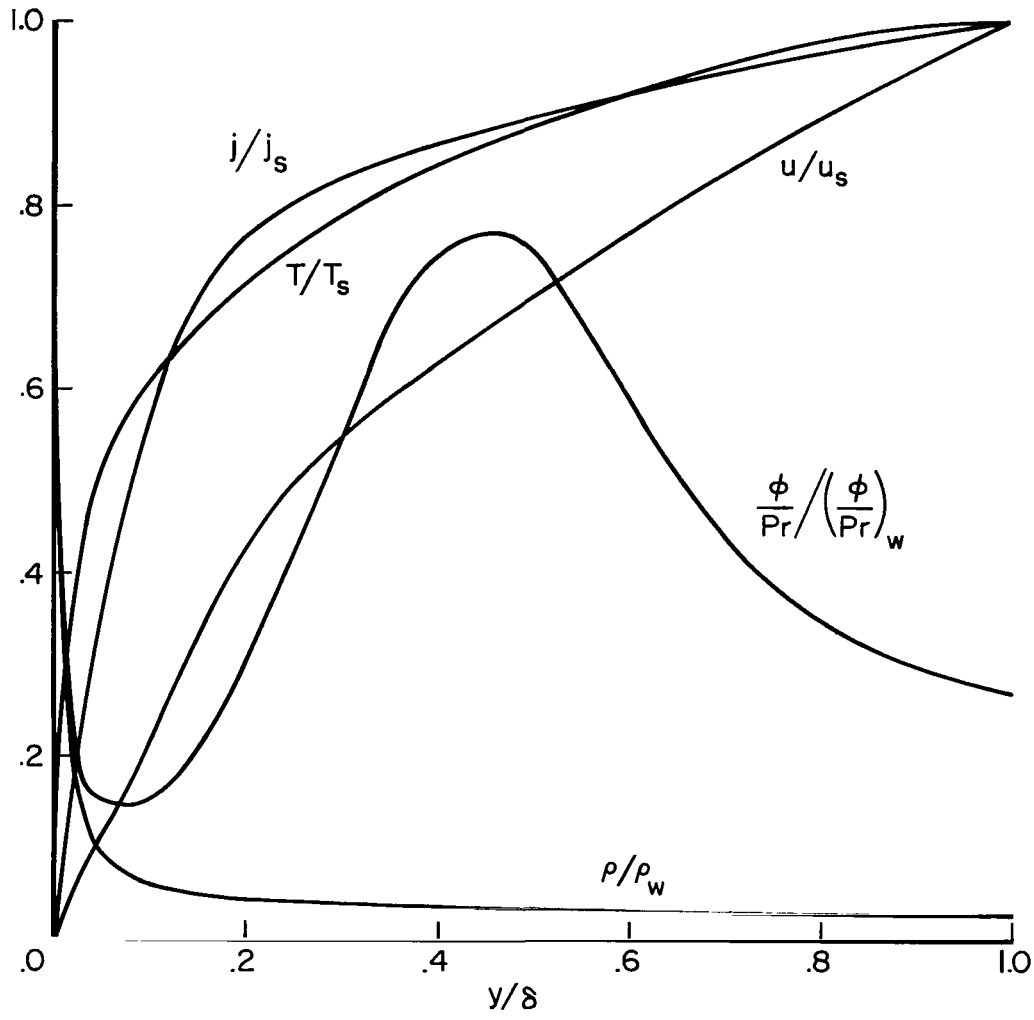

Figure 5.- Flow-field profiles for total thermal conductivity model II; U = 70,000 ft/sec, R = 0.25 ft, p_s = 1 atm, T_w = 3,000° K.

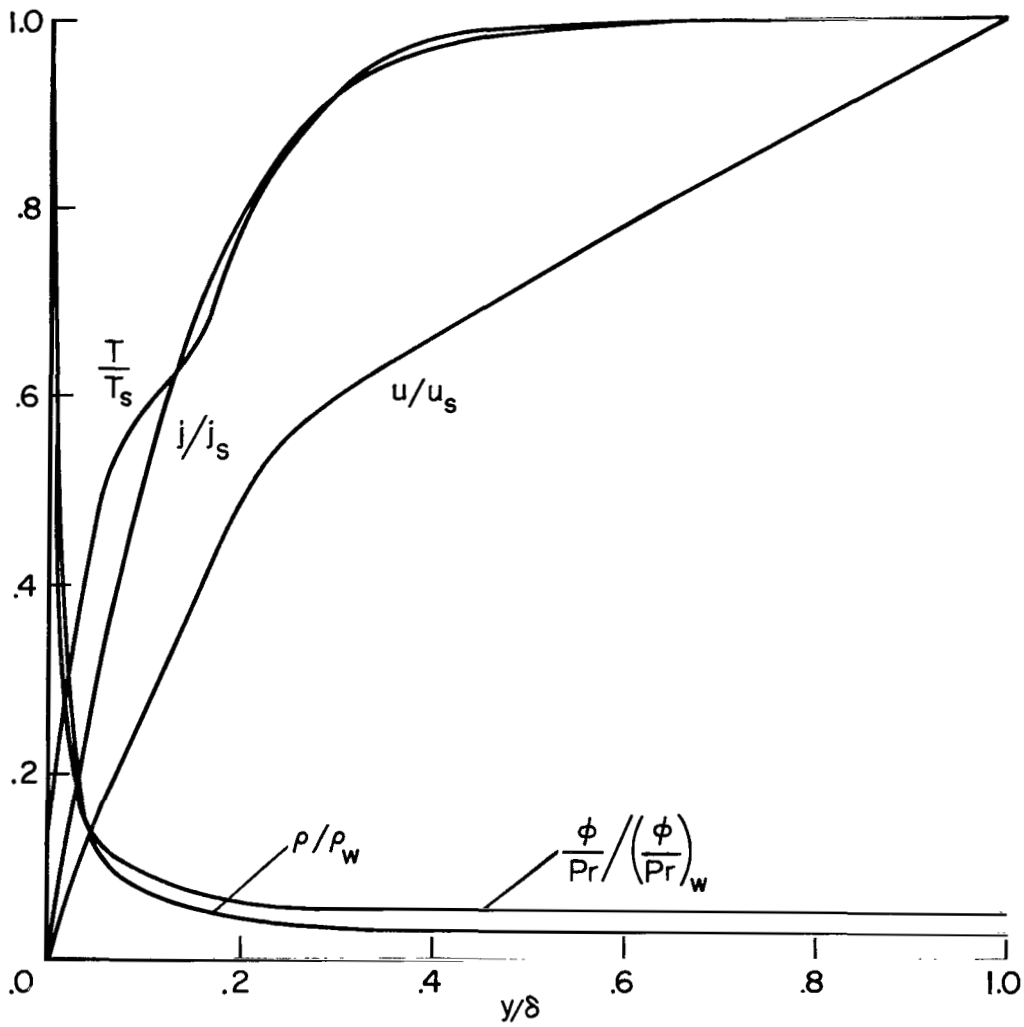

Figure 6.- Flow-field profiles for total thermal conductivity model III; U = 70,000 ft/sec, R = 0.25 ft, p_s = 1 atm, T_w = 3,000° K.

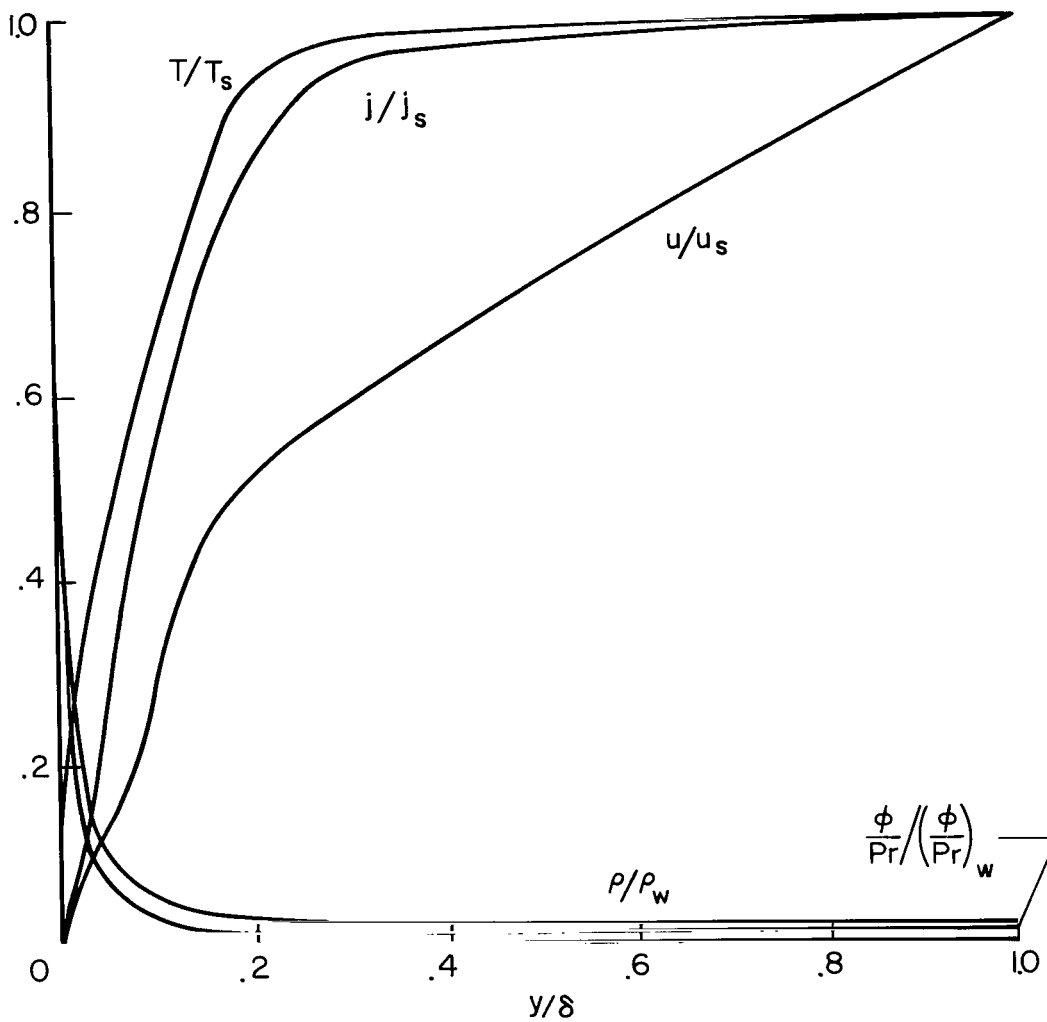

Figure 7.- Flow-field profiles for total thermal conductivity model I; U = 85,000 ft/sec, p_s = 1 atm, R = 0.25 ft, T_w = 3,000° K.

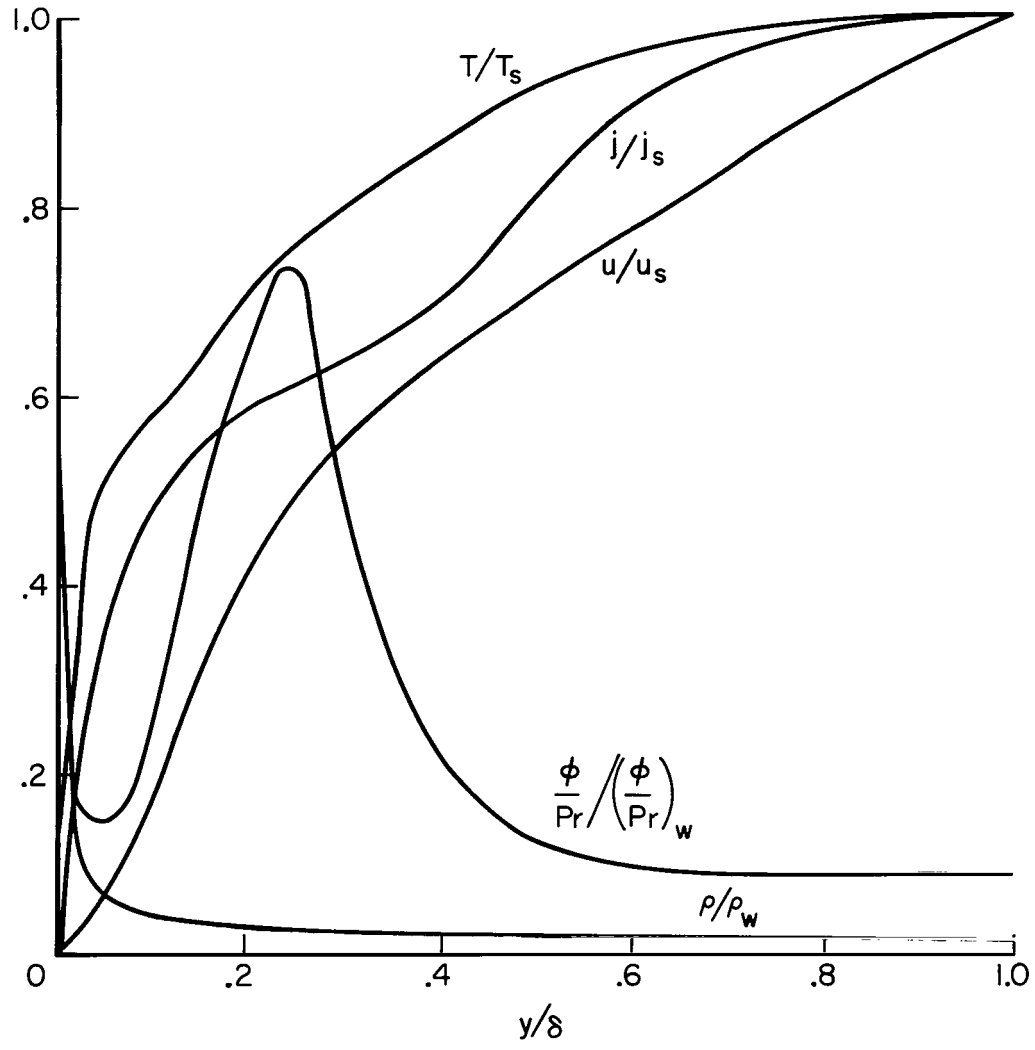

Figure 8.- Flow-field profiles for total thermal conductivity model II; U = 85,000 ft/sec, p_s = 1 atm, R = 0.25 ft, T_w = 3,000° K.

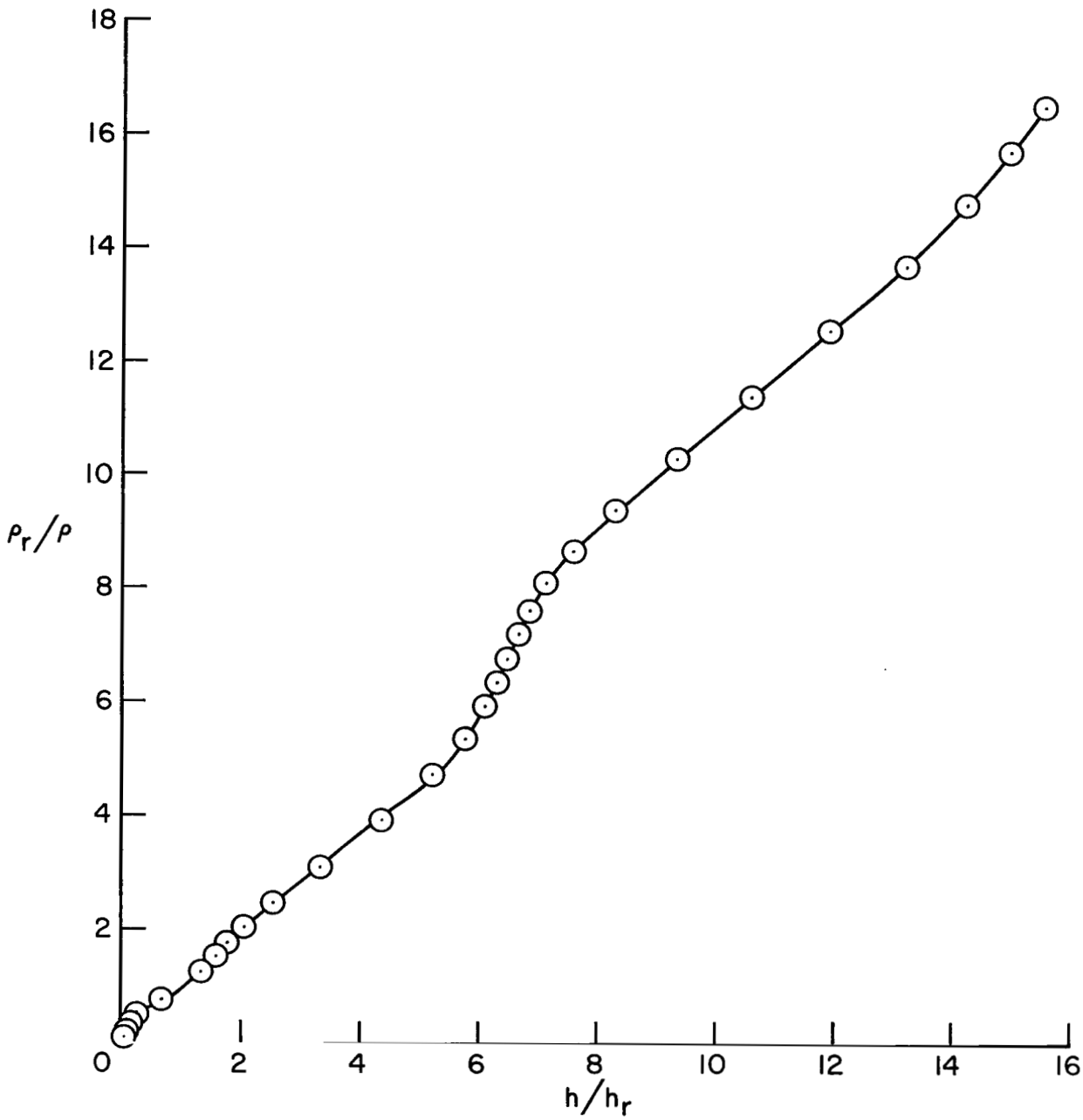

Figure 9.- Density correlation, p = 0.1 atm.

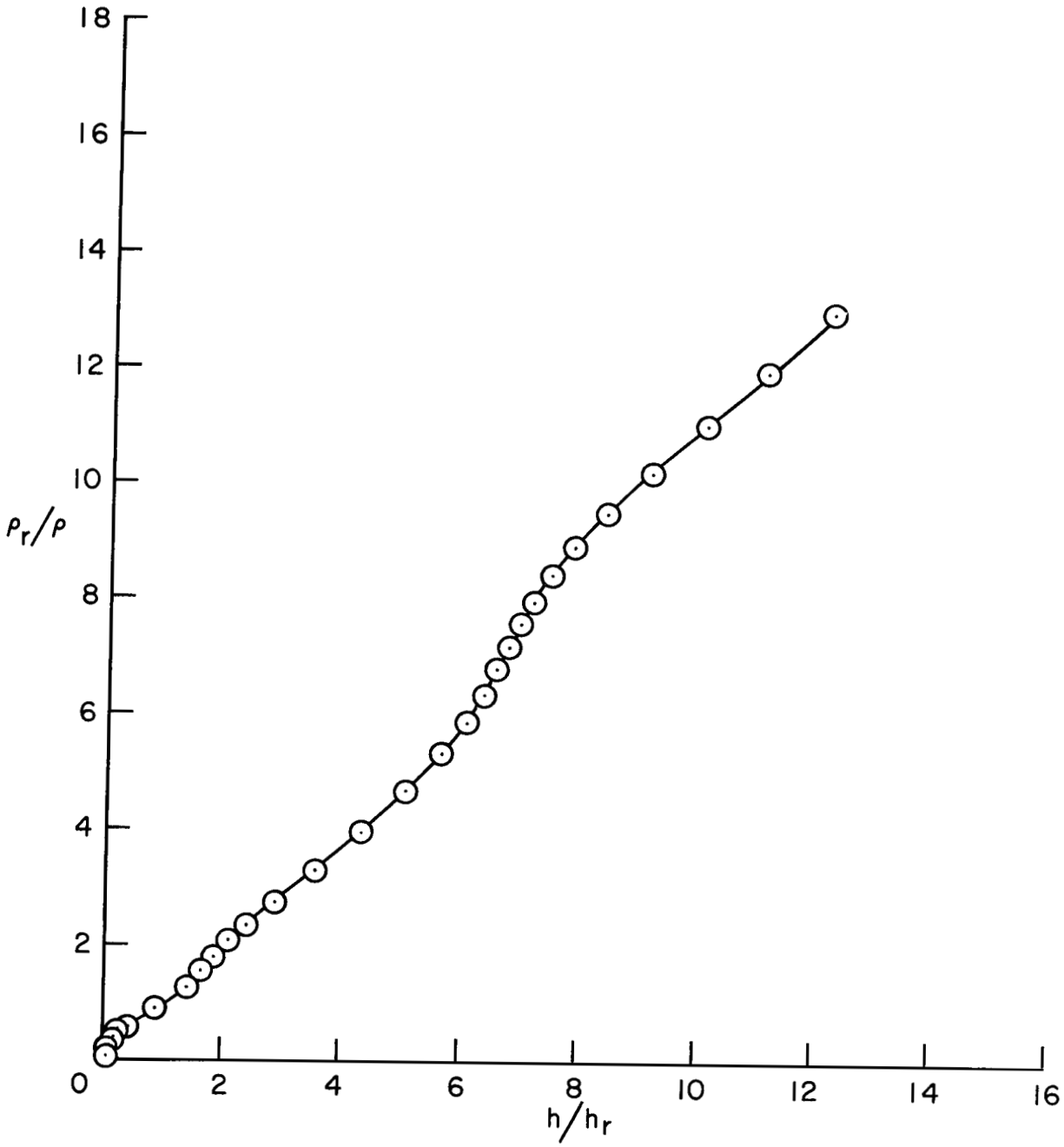

Figure 10.- Density correlation, p = 1 atm.

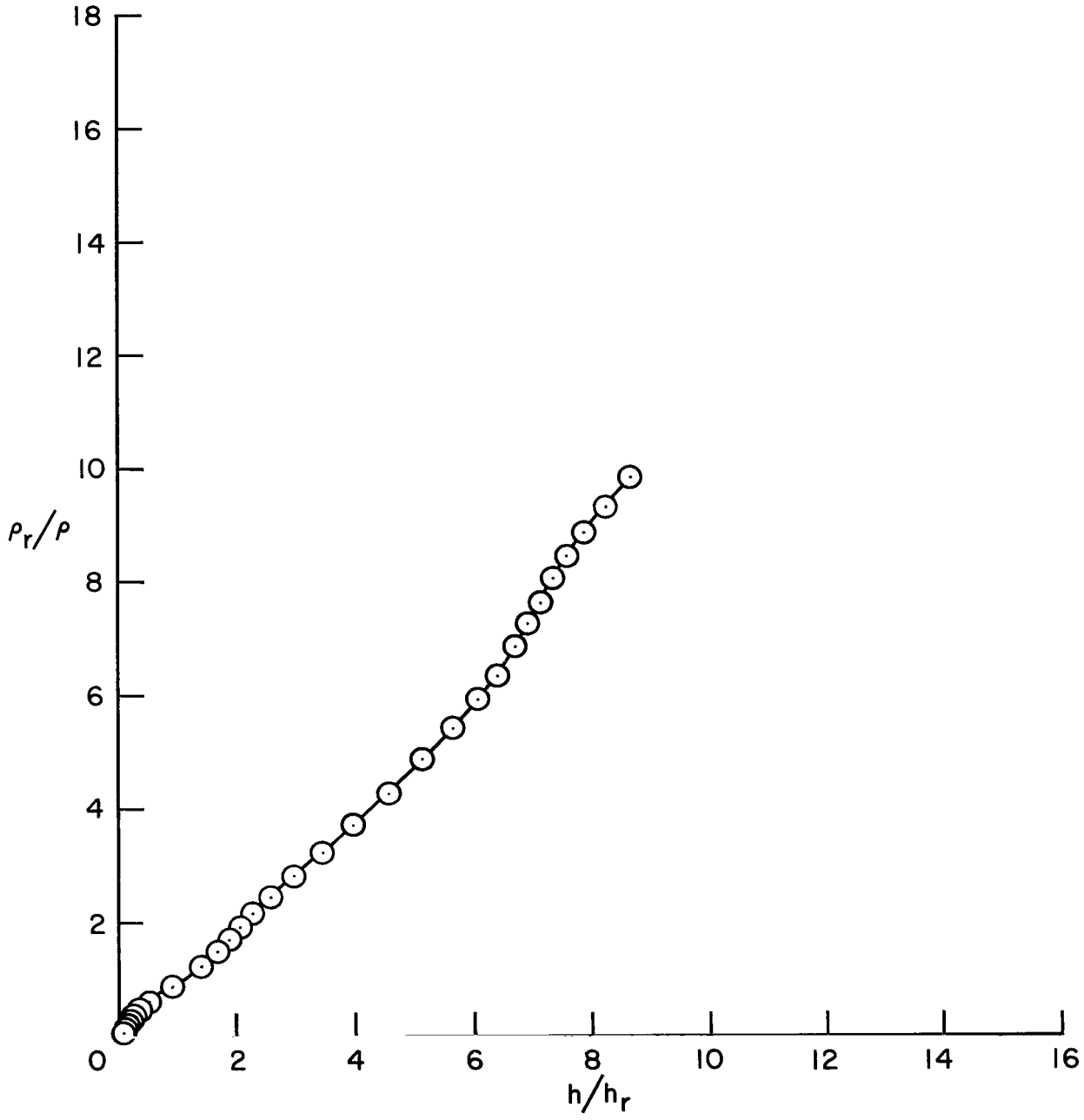

Figure 11.- Density correlation, p = 10 atm.

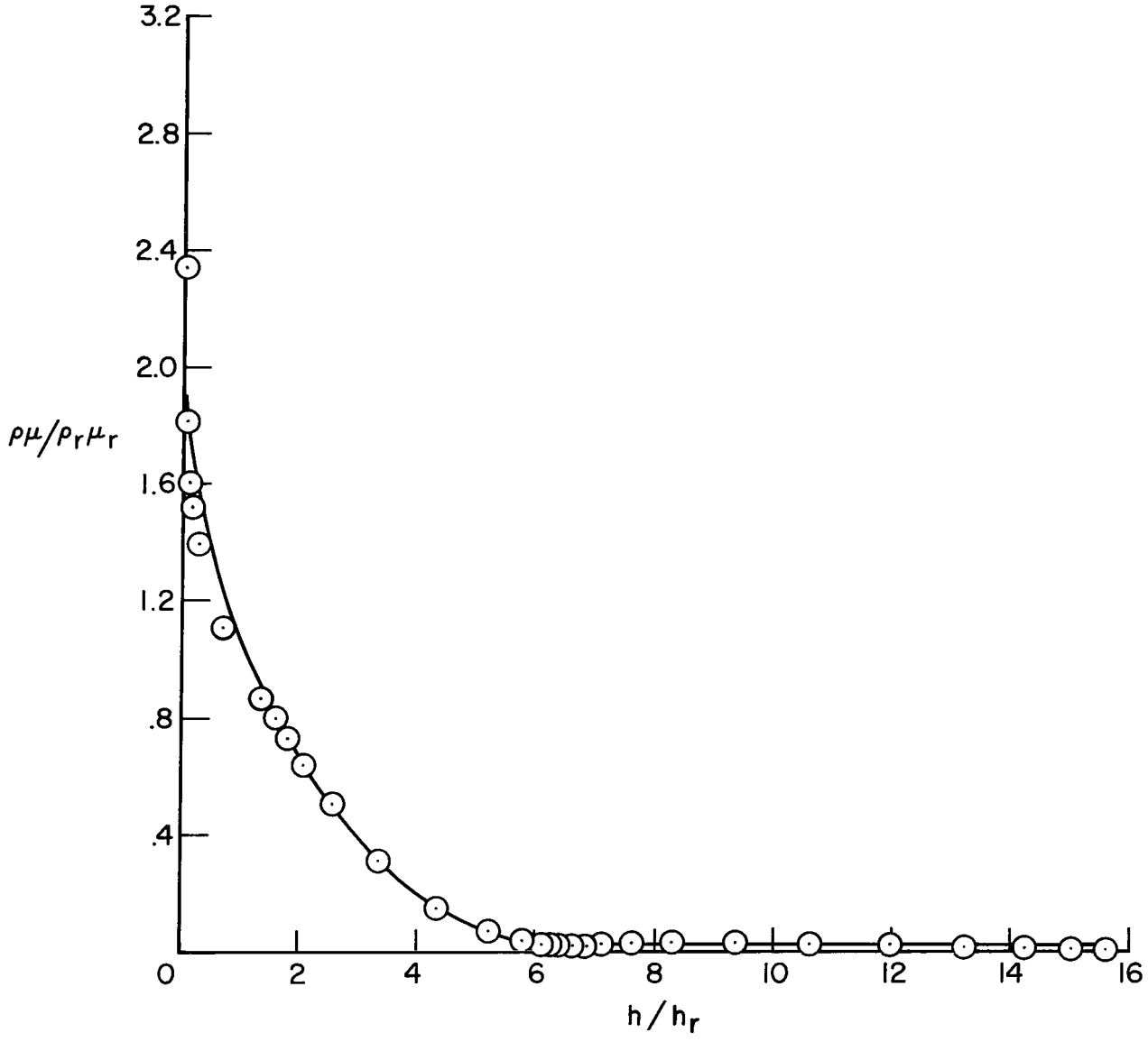

Figure 12.- Density-viscosity correlation, p = 0.1 atm.

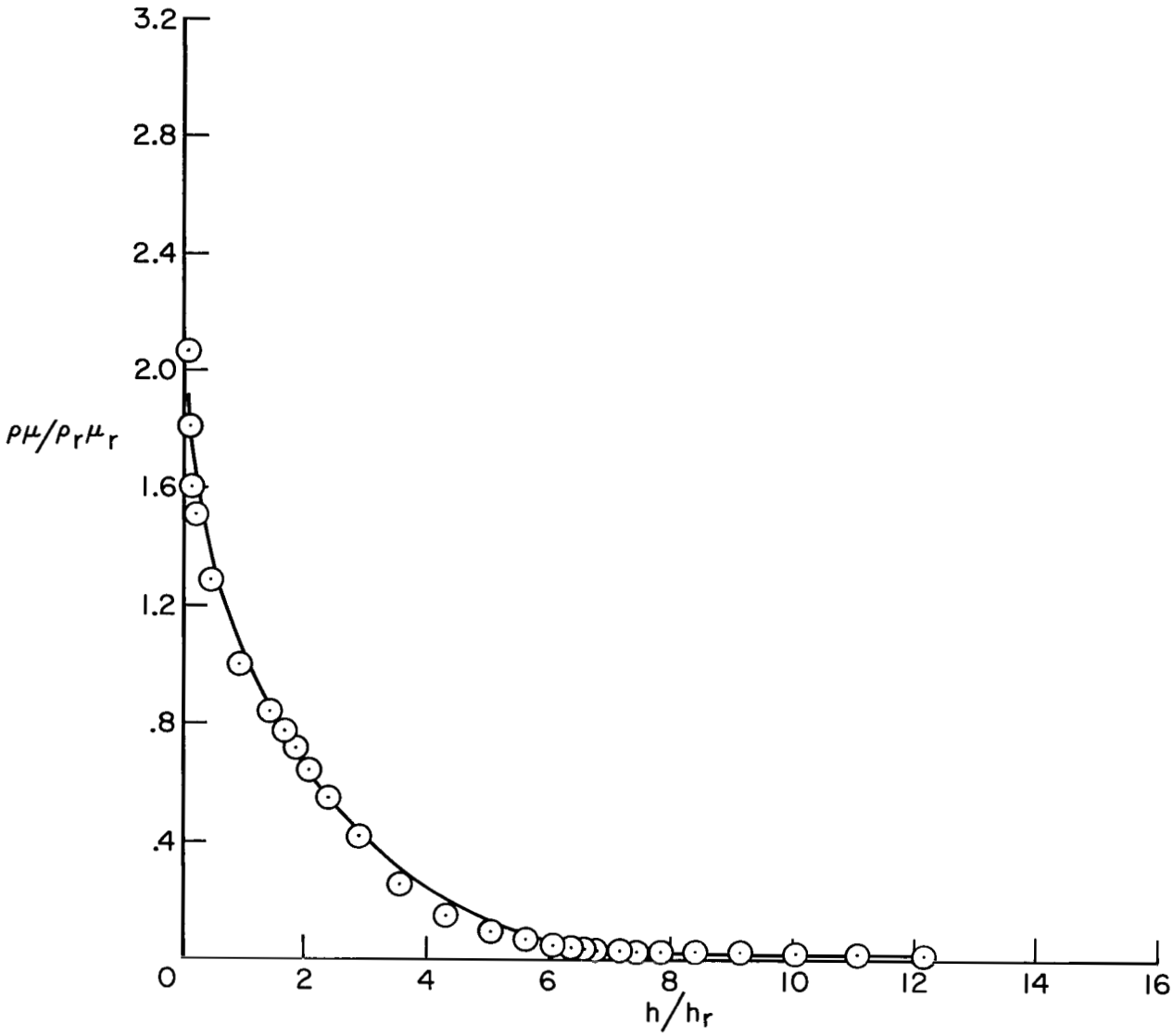

Figure 13.- Density-viscosity correlation, p = 1 atm.

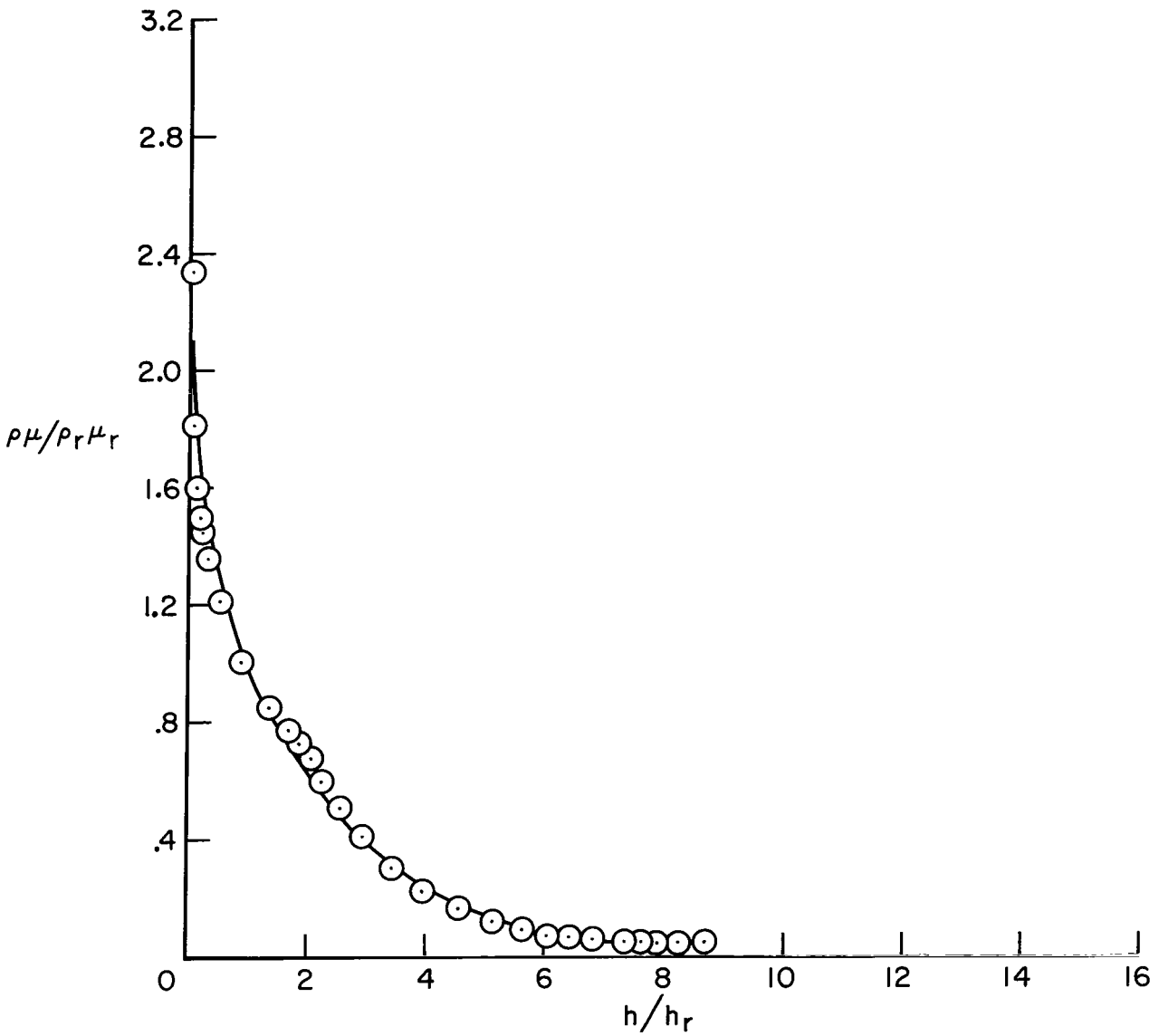

Figure 14.- Density-viscosity correlation, p = 10 atm.

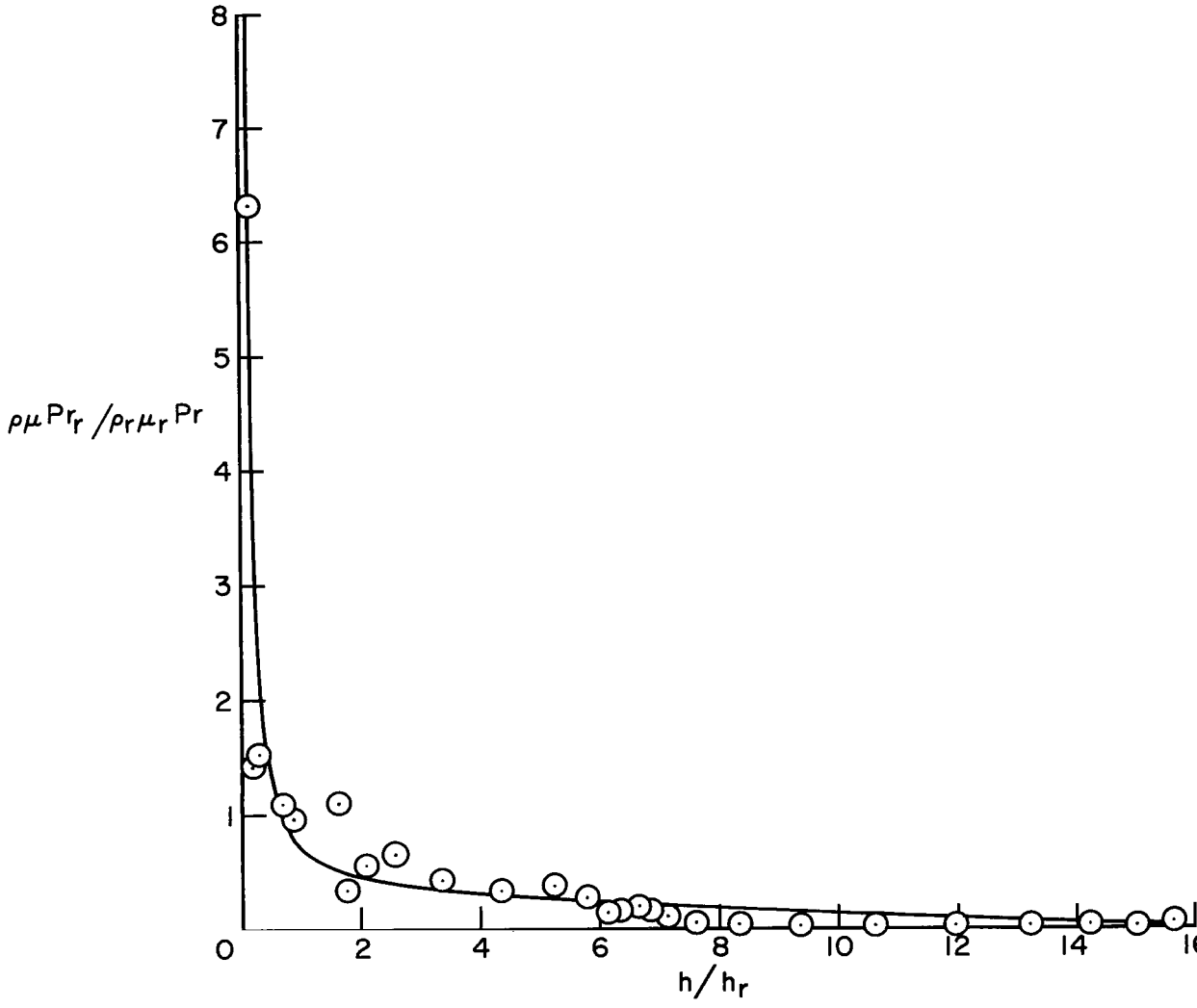

Figure 15.- Density-viscosity Prandtl number correlation, p = 0.1 atm.

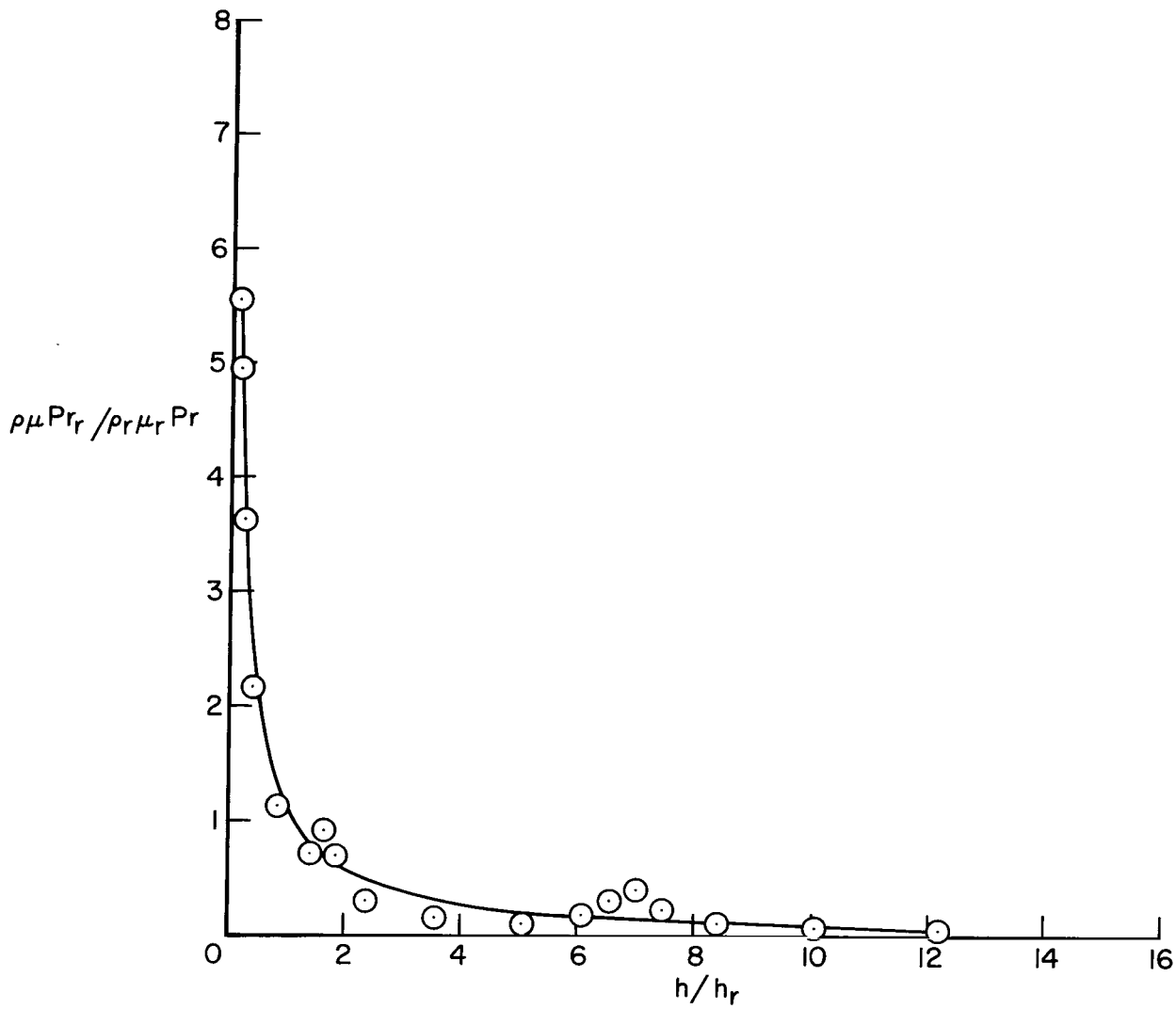

(a) Model I.

Figure 16.- Density-viscosity Prandtl number correlation, p = 1 atm.

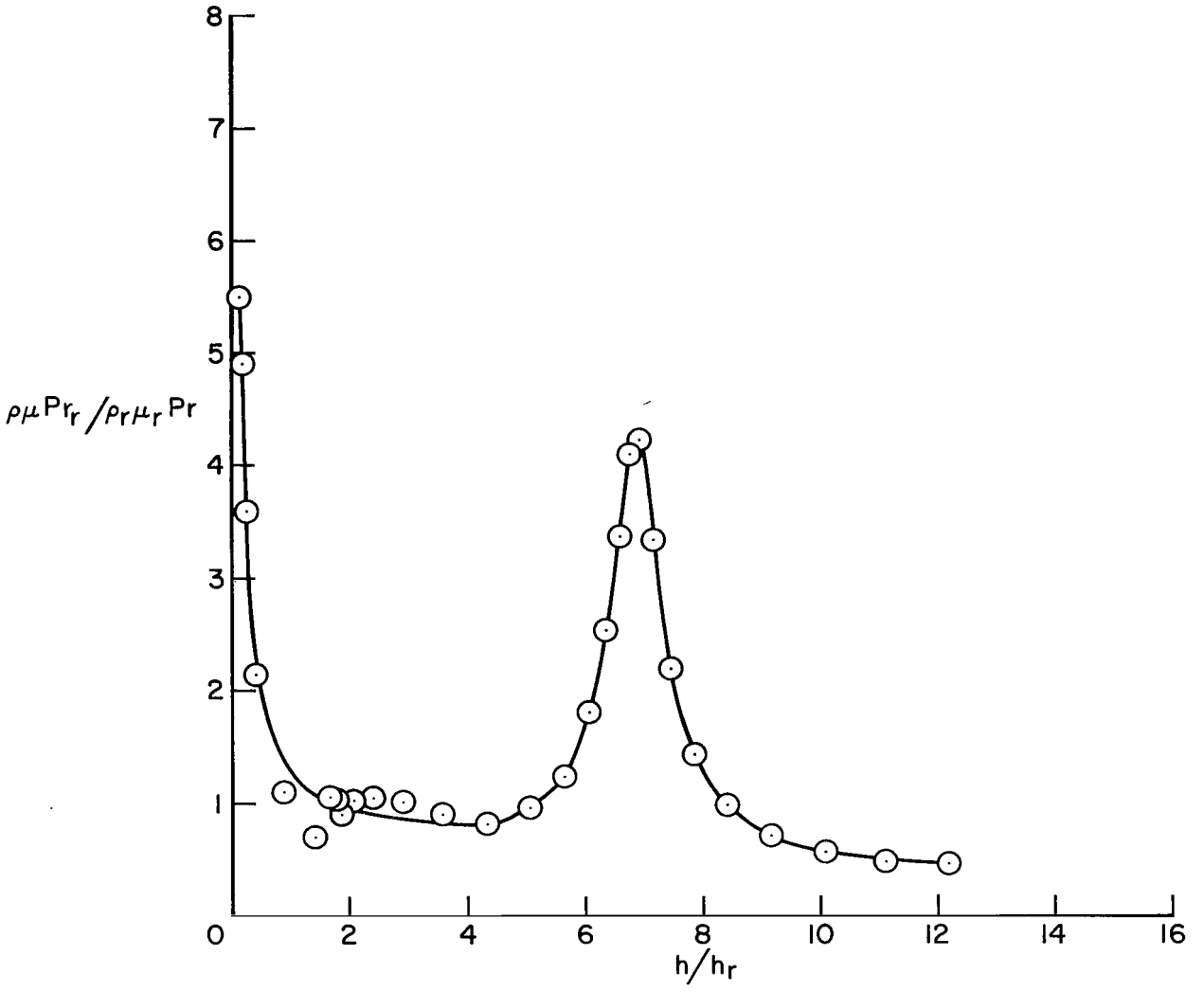

(b) Model II.

Figure 16.- Continued.

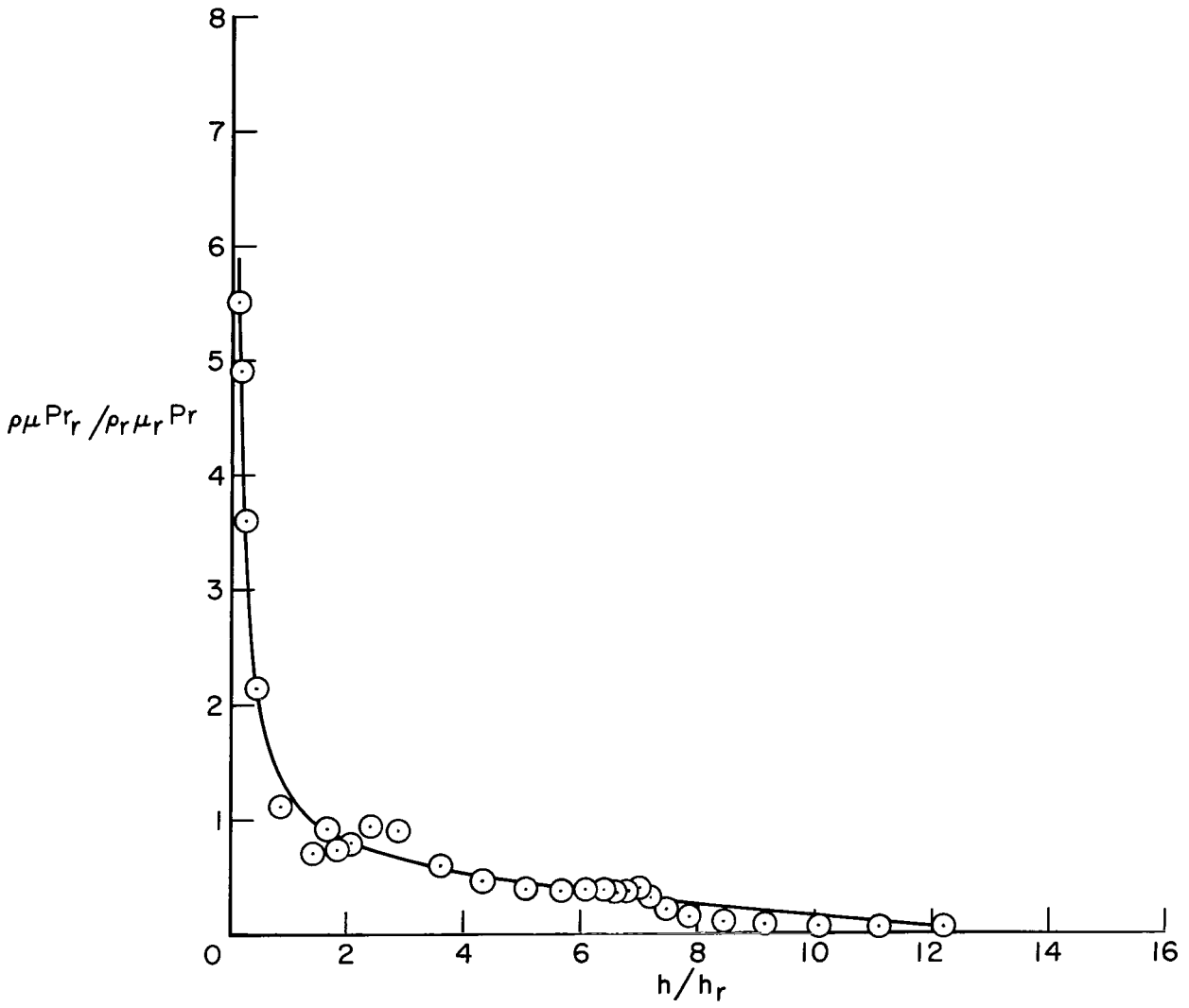

(c) Model III.

Figure 16.- Concluded.

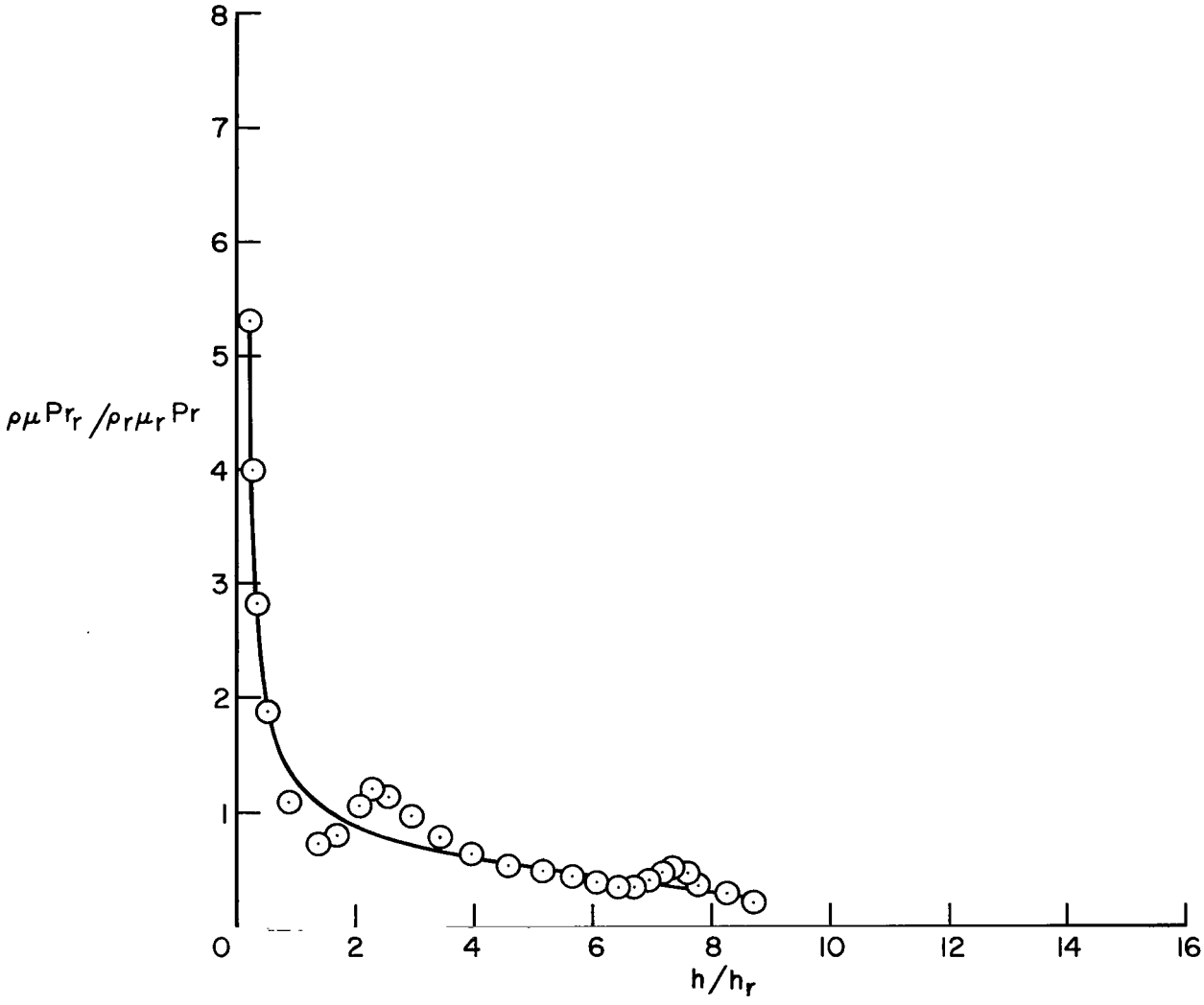

Figure 17.- Density-viscosity Prandtl number correlation, p = 10 atm.

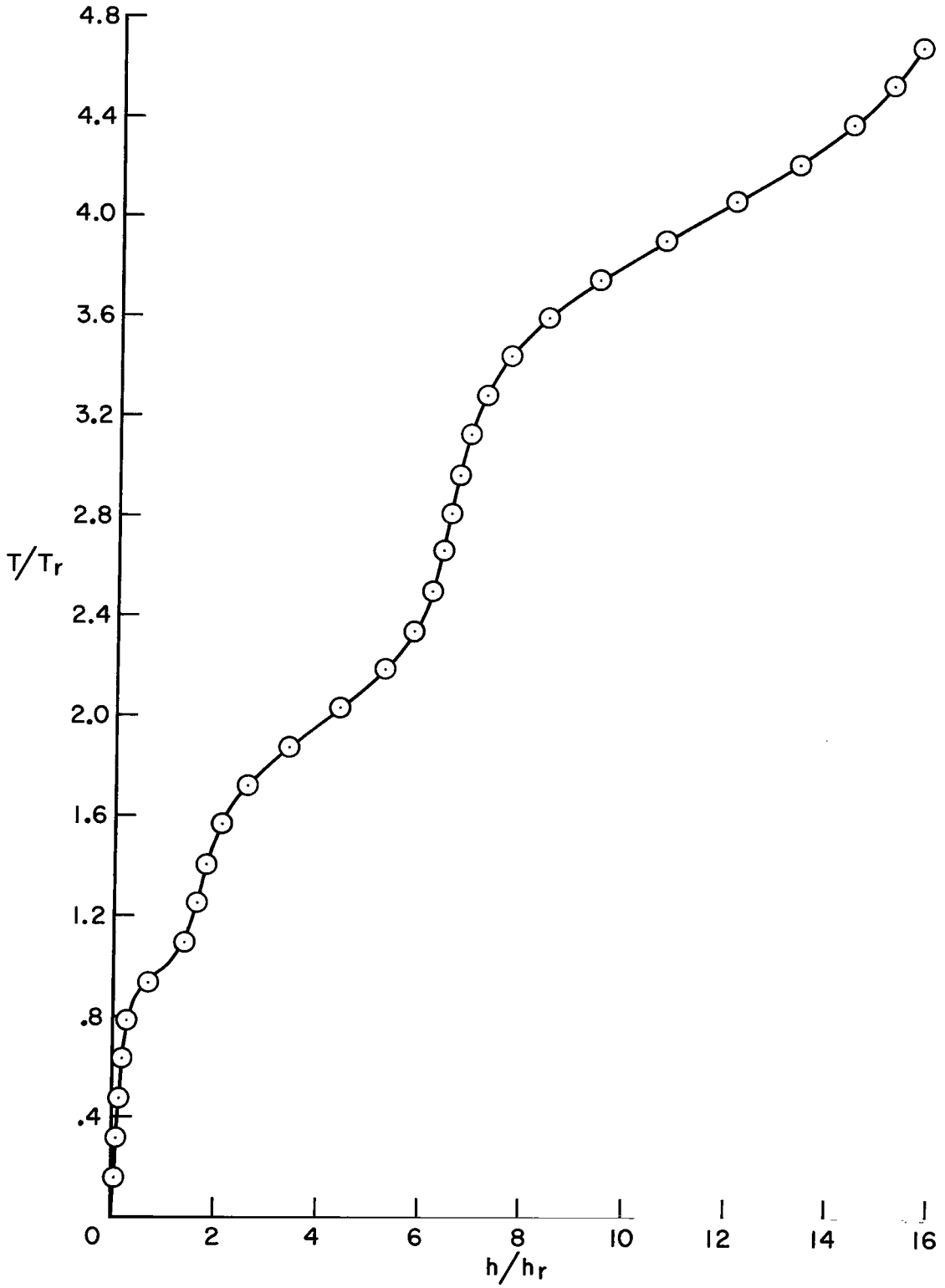

Figure 18.- Temperature correlation, p = 0.1 atm.

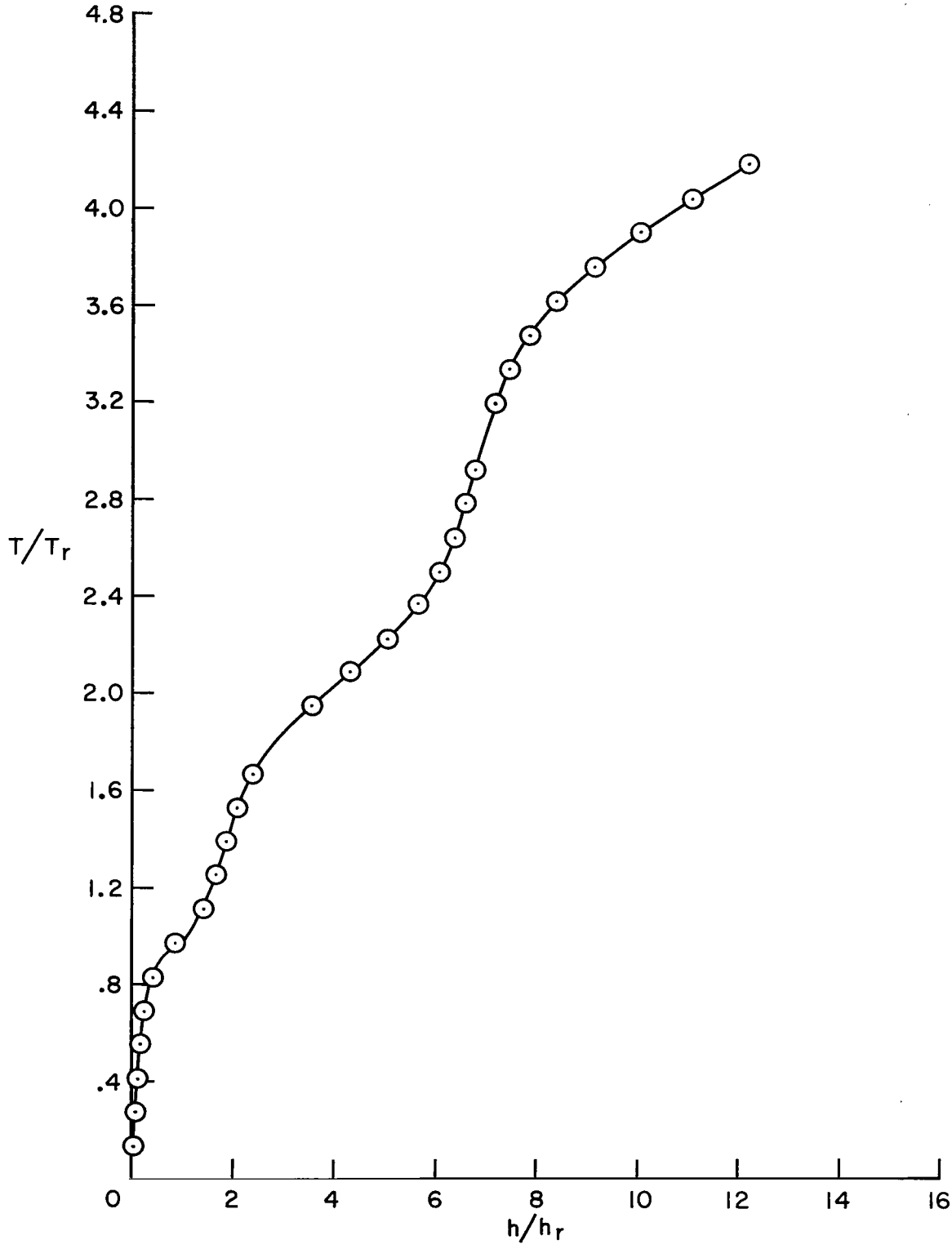

Figure 19.- Temperature correlation, p = 1.0 atm.

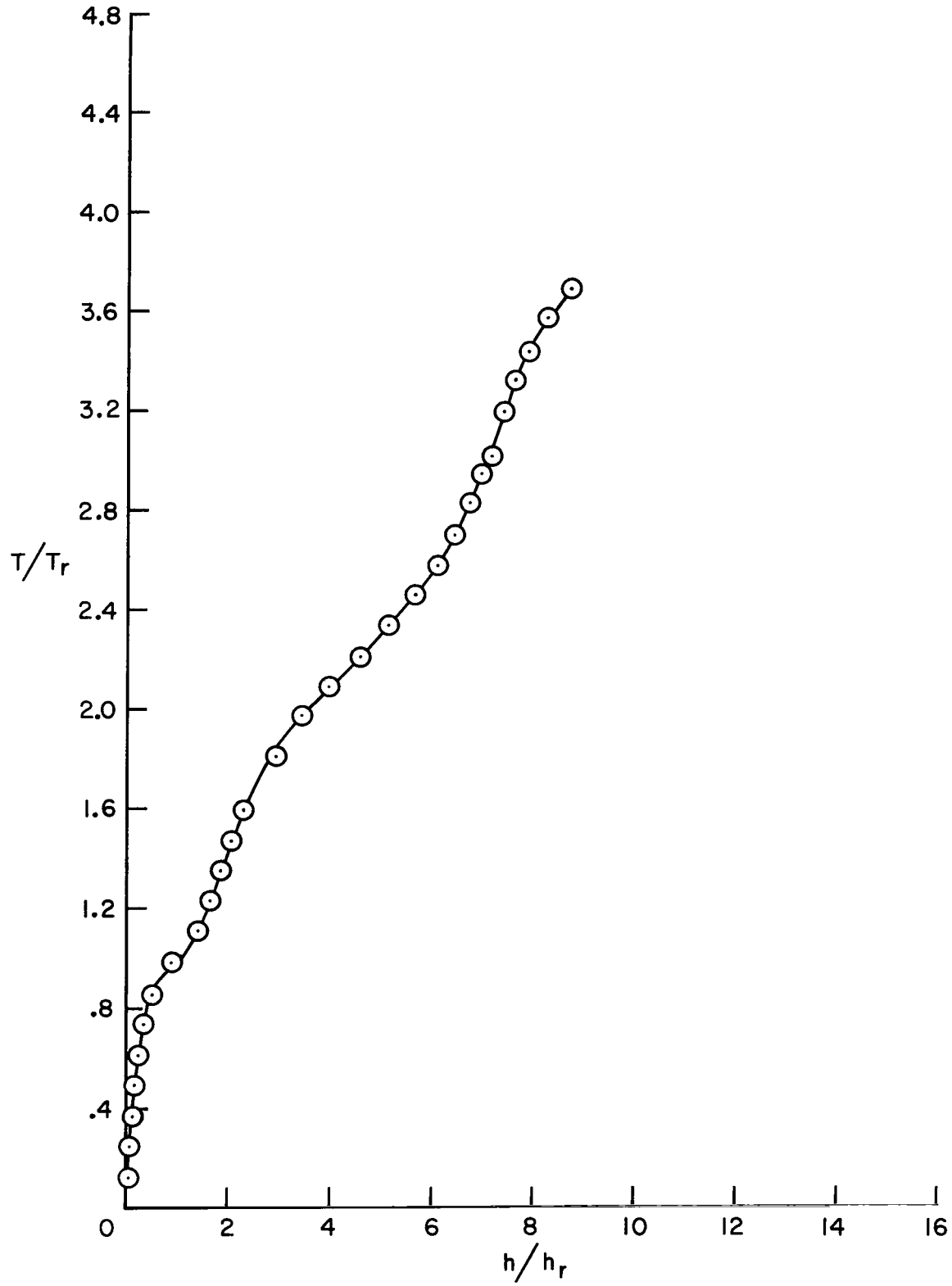

Figure 20.- Temperature correlation, p = 10 atm.

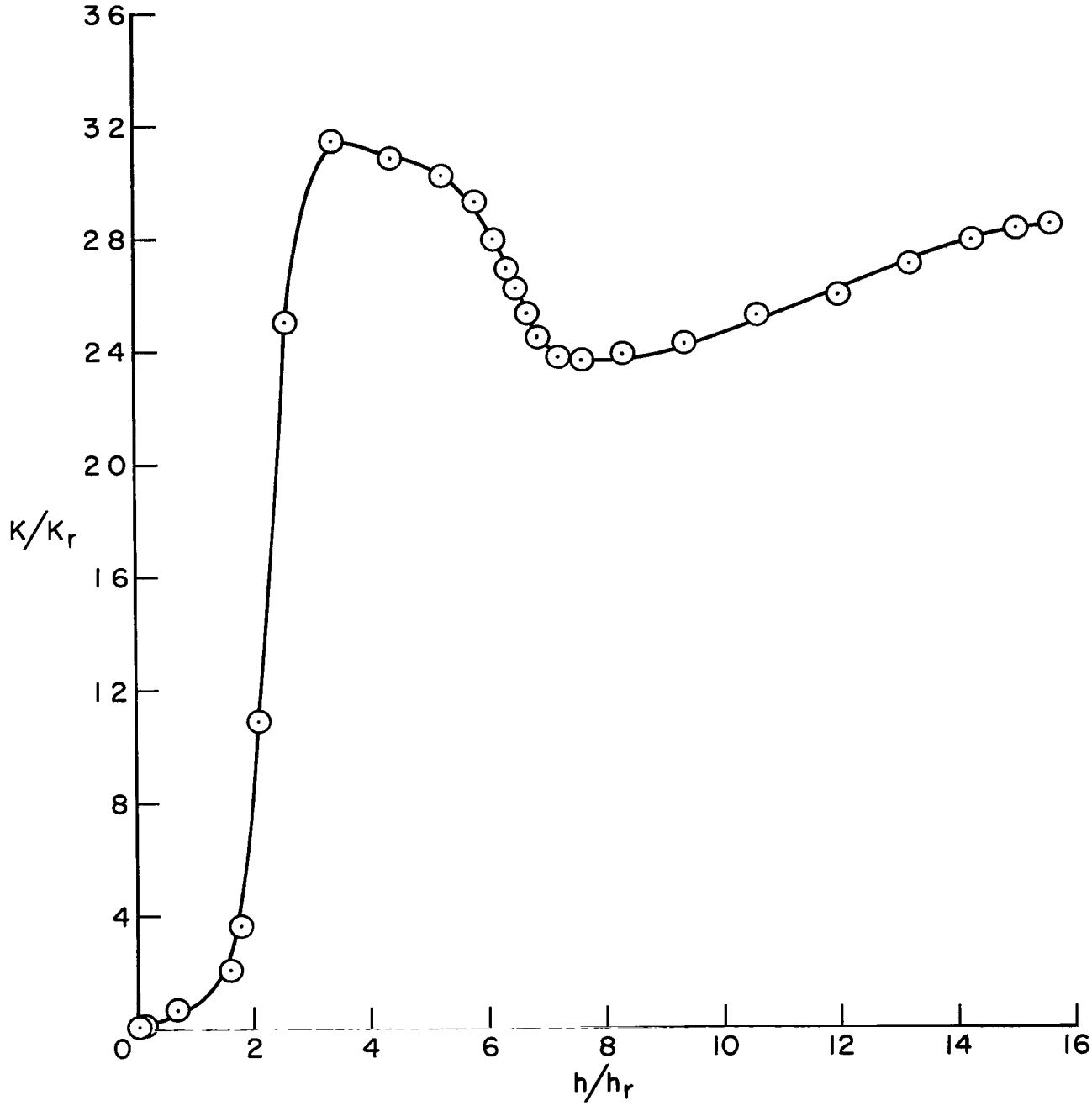

Figure 21.- Planck mean mass absorption coefficient, p = 0.1 atm.

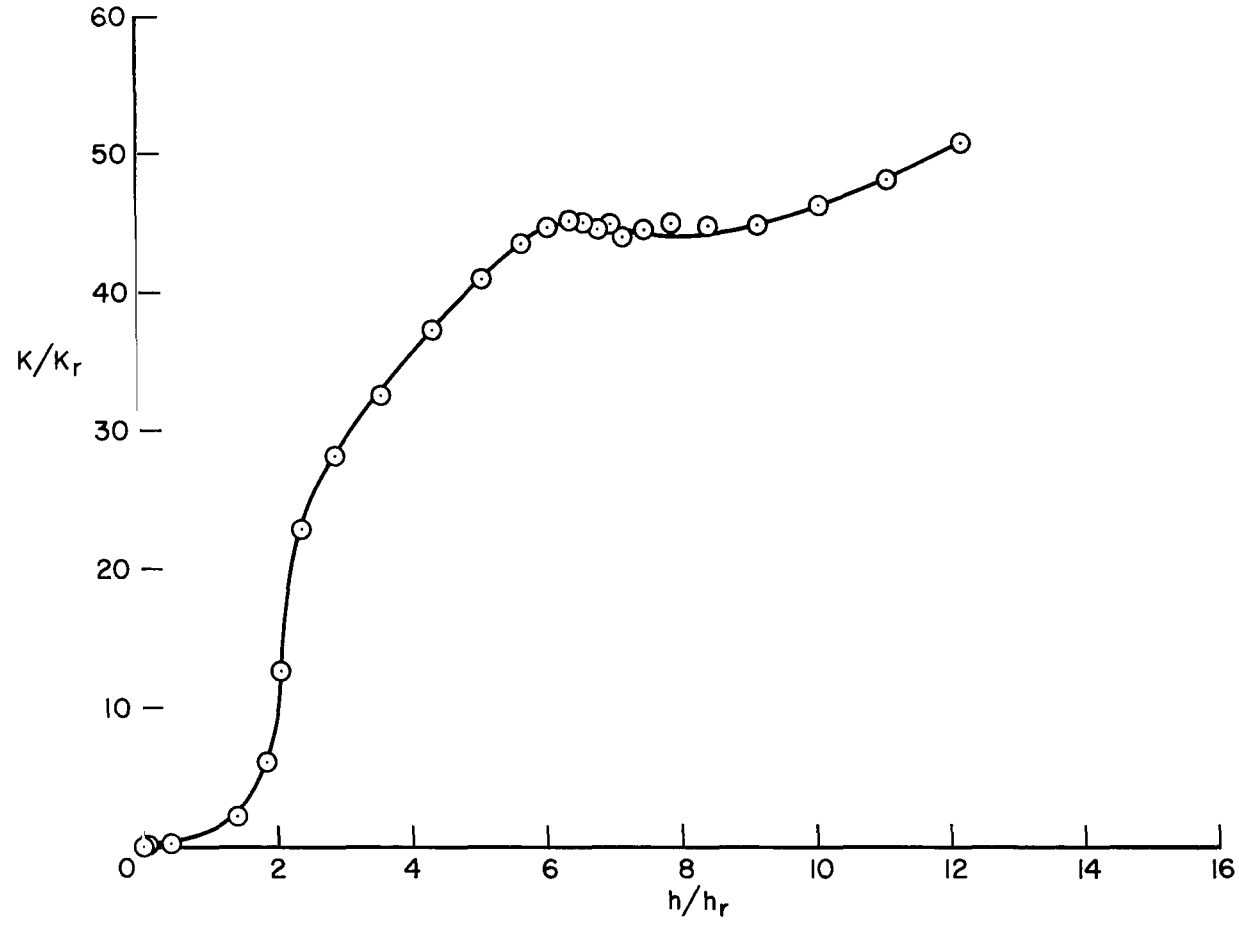

Figure 22.- Planck mean mass absorption coefficient, p = 1.0 atm.

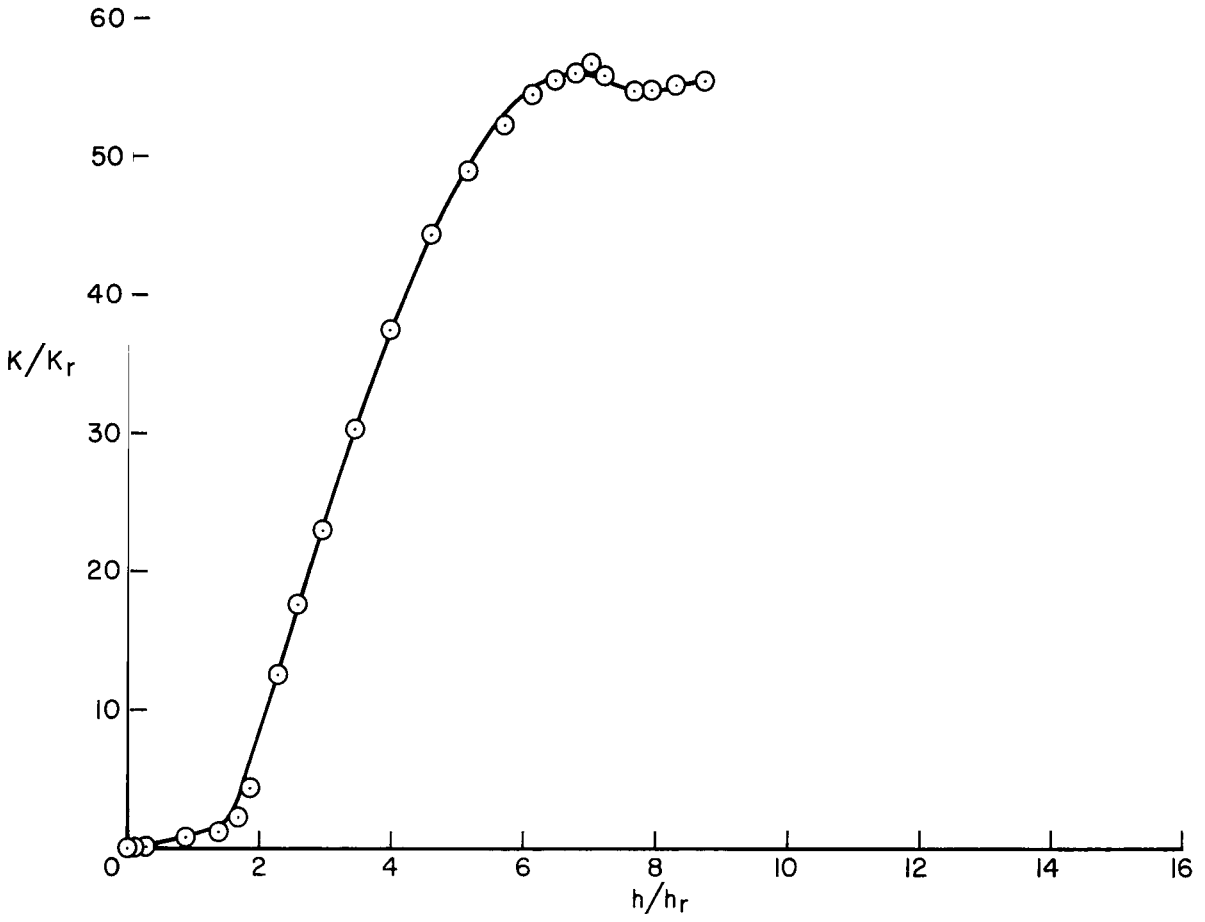

Figure 23.- Planck mean mass absorption coefficient, p = 10 atm.

2/22/85

"The aeronautical and space activities of the United States shall be conducted so as to contribute . . . to the expansion of human knowledge of phenomena in the atmosphere and space. The Administration shall provide for the widest practicable and appropriate dissemination of information concerning its activities and the results thereof."

—NATIONAL AERONAUTICS AND SPACE ACT OF 1958

NASA SCIENTIFIC AND TECHNICAL PUBLICATIONS

TECHNICAL REPORTS: Scientific and technical information considered important, complete, and a lasting contribution to existing knowledge.

TECHNICAL NOTES: Information less broad in scope but nevertheless of importance as a contribution to existing knowledge.

TECHNICAL MEMORANDUMS: Information receiving limited distribution because of preliminary data, security classification, or other reasons.

CONTRACTOR REPORTS: Technical information generated in connection with a NASA contract or grant and released under NASA auspices.

TECHNICAL TRANSLATIONS: Information published in a foreign language considered to merit NASA distribution in English.

TECHNICAL REPRINTS: Information derived from NASA activities and initially published in the form of journal articles.

SPECIAL PUBLICATIONS: Information derived from or of value to NASA activities but not necessarily reporting the results of individual NASA-programmed scientific efforts. Publications include conference proceedings, monographs, data compilations, handbooks, sourcebooks, and special bibliographies.

Details on the availability of these publications may be obtained from:

SCIENTIFIC AND TECHNICAL INFORMATION DIVISION

NATIONAL AERONAUTICS AND SPACE ADMINISTRATION

Washington, D.C. 20546